Article

Cell Host & Microbe

Cross-regulation of antibody responses against the SARS-CoV-2 Spike protein and commensal microbiota via molecular mimicry

Graphical abstract

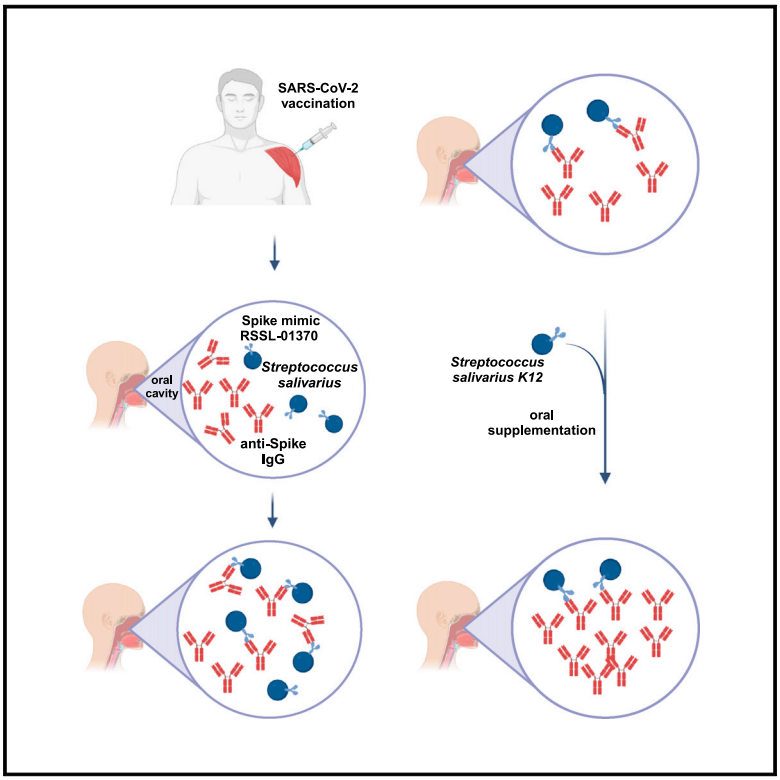

Highlights

- SARS-CoV-2 vaccination induces an early increase in *S. salivarius* in the oral cavity
- Anti-Spike-SARS-CoV-2 antibodies bind to *S. salivarius* via molecular mimicry
- *S. salivarius* induces cross-reactive anti-Spike Abs in mice, aiding virus clearance
- *S. salivarius* boosts salivary anti-Spike antibodies in the vaccinees

Authors

Marina Bondareva, Lisa Budzinski, Pawel Durek, ..., Philipp Enghard, Mir-Farzin Mashreghi, Andrey A. Kruglov

Correspondence

kruglov@drfz.de

In brief

Bondareva et al. show that commensal bacteria, including *Streptococcus salivarius*, trigger cross-reactive anti-Spike antibodies capable of SARS-CoV-2 virus inhibition. *Streptococcus salivarius* abundance correlates with salivary anti-Spike antibodies early after SARS-CoV-2 vaccination. *Streptococcus salivarius* supplementation enhances salivary anti-Spike antibodies in vaccinees.

Bondareva et al., 2023, Cell Host & Microbe *31*, 1866–1881
November 8, 2023
https://doi.org/10.1016/j.chom.2023.10.007

CellPress

CellPress
OPEN ACCESS

Cell Host & Microbe

Article

Cross-regulation of antibody responses against the SARS-CoV-2 Spike protein and commensal microbiota via molecular mimicry

Marina Bondareva,[1,2,23] Lisa Budzinski,[1,23] Pawel Durek,[1,23] Mario Witkowski,[3,4,5,23] Stefan Angermair,[6,23] Justus Ninnemann,[1,23] Jakob Kreye,[3,7,8,9,10] Philine Letz,[1] Marta Ferreira-Gomes,[1] Iaroslav Semin,[1,2] Gabriela Maria Guerra,[1] S. Momsen Reincke,[3,7,8,9] Elisa Sánchez-Sendin,[7,8,9] Selin Yilmaz,[1] Toni Sempert,[1] Gitta Anne Heinz,[1] Caroline Tizian,[3,4,5] Martin Raftery,[11] Günther Schönrich,[11] Daria Matyushkina,[12] Ivan V. Smirnov,[13] Vadim M. Govorun,[12] Eva Schrezenmeier,[3,14] Anna-Luisa Stefanski,[1,15] Thomas Dörner,[1,15] Silvia Zocche,[16]

(Author list continued on next page)

[1]Deutsches Rheuma-Forschungszentrum (DRFZ), an Institute of the Leibniz Association, 10117 Berlin, Germany
[2]Belozersky Institute of Physico-Chemical Biology and Faculty of Bioengineering and Bioinformatics, M.V. Lomonosov Moscow State University, 119234 Moscow, Russia
[3]Berlin Institute of Health (BIH), 10178 Berlin, Germany
[4]Laboratory of Innate Immunity, Department of Microbiology and Infection Immunology, Charité-Universitätsmedizin Berlin, 12203 Berlin, Germany
[5]Mucosal and Developmental Immunology, Deutsches Rheuma-Forschungszentrum, an Institute of the Leibniz Association, 10117 Berlin, Germany
[6]Charité-Universitätsmedizin Berlin, corporate member of Freie Universität Berlin and Humboldt Universität zu Berlin, Department of Anesthesiology and Intensive Care Medicine, Charité Campus Benjamin Franklin, Berlin, Germany
[7]German Center for Neurodegenerative Diseases (DZNE), 10117 Berlin, Germany
[8]Helmholtz Innovation Lab BaoBab (Brain Antibody-omics and B-cell Lab), 10117 Berlin, Germany
[9]Department of Neurology and Experimental Neurology, Charité-Universitätsmedizin Berlin, corporate member of Freie Universität Berlin and Humboldt-Universität Berlin, and Berlin Institute of Health, 10117 Berlin, Germany
[10]Department of Pediatric Neurology, Charité-Universitätsmedizin Berlin, corporate member of Freie Universität Berlin and Humboldt-Universität Berlin, and Berlin Institute of Health, 10117 Berlin, Germany
[11]Institute of Virology, Charité-Universitätsmedizin Berlin, corporate member of Freie Universität Berlin and Humboldt-Universität zu Berlin, and Berlin Institute of Health, Berlin, Germany

(Affiliations continued on next page)

SUMMARY

The commensal microflora provides a repertoire of antigens that illicit mucosal antibodies. In some cases, these antibodies can cross-react with host proteins, inducing autoimmunity, or with other microbial antigens. We demonstrate that the oral microbiota can induce salivary anti-SARS-CoV-2 Spike IgG antibodies via molecular mimicry. Anti-Spike IgG antibodies in the saliva correlated with enhanced abundance of *Streptococcus salivarius* 1 month after anti-SARS-CoV-2 vaccination. Several human commensal bacteria, including *S. salivarius*, were recognized by SARS-CoV-2-neutralizing monoclonal antibodies and induced cross-reactive anti-Spike antibodies in mice, facilitating SARS-CoV-2 clearance. A specific *S. salivarius* protein, RSSL-01370, contains regions with homology to the Spike receptor-binding domain, and immunization of mice with RSSL-01370 elicited anti-Spike IgG antibodies in the serum. Additionally, oral *S. salivarius* supplementation enhanced salivary anti-Spike antibodies in vaccinated individuals. Altogether, these data show that distinct species of the human microbiota can express molecular mimics of SARS-CoV-2 Spike protein, potentially enhancing protective immunity.

INTRODUCTION

SARS-CoV-2 infects cells via the interaction of the Spike (S) protein with the angiotensin converting enzyme 2 (ACE2) receptor, which is expressed by various cell types.[1–3] The S protein of SARS-CoV-2 contains a receptor-binding domain (RBD) that mediates its interaction with ACE2 and promotes viral entry.[3,4] Blocking of this crucial interaction by monoclonal

CellPress
OPEN ACCESS

Edoardo Viviano,[17] Nele Klement,[14] Katharina Johanna Sehmsdorf,[14] Alexander Lunin,[18] Hyun-Dong Chang,[1,19] Marina Drutskaya,[20] Liubov Kozlovskaya,[18,21] Sascha Treskatsch,[6] Andreas Radbruch,[1,15] Andreas Diefenbach,[3,4,5] Harald Prüss,[7,8,9] Philipp Enghard,[14] Mir-Farzin Mashreghi,[1,24,25] and Andrey A. Kruglov[1,2,20,22,24,25,26,*]

[12]Scientific Research Institute for Systems Biology and Medicine, Scientific Driveway, 18, 117246 Moscow, Russia
[13]Shemyakin-Ovchinnikov Institute of Bioorganic Chemistry, Russian Academy of Sciences, Moscow 117997, Russia
[14]Department of Nephrology and Intensive Care Medicine, Charité-Universitätsmedizin Berlin, corporate member of Freie Universität Berlin and Humboldt-Universität zu Berlin, and Berlin Institute of Health, 10117 Berlin, Germany
[15]Department of Rheumatology and Clinical Immunology, Charité-Universitätsmedizin Berlin, corporate member of Freie Universität Berlin and Humboldt-Universität zu Berlin, Berlin, Germany
[16]Departments of Pediatric Gastroenterology, Nephrology and Metabolic Diseases, Charité University Medicine, 10117 Berlin, Germany
[17]Charité-Universitätsmedizin Berlin, corporate member of Freie Universität Berlin and Humboldt-Universität zu Berlin and Berlin Institute of Health, Institute of Physiology, Center for Space Medicine and Extreme Environments Berlin, 10117 Berlin, Germany
[18]Chumakov Scientific Center for Research and Development of Immune-and-Biological Products, Russian Academy of Sciences (Institute of Poliomyelitis), 108819 Moscow, Russia
[19]Institute of Biotechnology, Technische Universität Berlin, Berlin, Germany
[20]Center for Precision Genome Editing and Genetic Technologies for Biomedicine, Engelhardt Institute of Molecular Biology, Russian Academy of Sciences, 119991 Moscow, Russia
[21]Institute for Translational Medicine and Biotechnology, Sechenov First Moscow State Medical University (Sechenov University), Moscow, Russia
[22]Biological Faculty, M.V. Lomonosov Moscow State University, 119234 Moscow, Russia
[23]These authors contributed equally
[24]These authors contributed equally
[25]Senior author
[26]Lead contact
*Correspondence: kruglov@drfz.de
https://doi.org/10.1016/j.chom.2023.10.007

anti-SARS-CoV-2-RBD antibodies (Abs) confers protection of the host against infection of target cells.[5,6] Systemic Abs in the blood (mainly IgG, IgM, and IgA1) curtail virus propagation after infection of the host, whereas the presence of antigen-specific Abs at the mucosal surfaces (IgA2, IgA1, and IgM) is required to prevent initial infection of the host.[7] Although systemic vaccination with a mRNA vaccine encoding the S protein of SARS-CoV-2 is known to induce anti-S Abs in the nasopharyngeal fluid, these Abs are not maintained for a long time,[8] and the mechanisms ensuring the maintenance of salivary anti-SARS-CoV-2 Ab responses are poorly understood.

Secretion of Abs at mucosal surfaces can be enhanced by antigens presented by the mucosal microbiota.[9] It is estimated that the human microbiota contains several millions of genes,[10] thus potentially providing a plethora of epitopes for Ab binding.[11] Some of these epitopes may resemble host proteins, potentially inducing cross-reactive autoimmunity,[12–16] whereas others may mimic proteins from different microorganisms and provide cross-protective immunity.[12,17] Microbiota-induced immunity is known to provide protection against microbial infections by *Citrobacter rodentium*, *Clostridiodes difficile*, *Pseudomonas aeruginosa*[18–20] and by viruses such as influenza.[21] Protection is mediated by increasing the fitness of the innate immune system via tonic type I interferon (IFN) production[22,23] and by cross-reactive Ab responses.[18] Interestingly, cross-reactive Abs targeting glycoprotein (gp)41 of HIV-1 are induced by distinct commensal microbiota.[24] Furthermore, such microbiota-induced gp41 reactive B cells diverted the Ab response generated by vaccination using envelope (Env) glycoprotein to non-neutralizing epitopes on HIV-1 Env.[25]

Several studies have reported the presence of SARS-CoV-2-RBD Abs in unexposed healthy individuals.[26–30] Induction of such Abs in previous infections with common cold coronaviruses has been postulated, but this link has not been formally proven. The original antigens inducing cross-reactive RBD secretory IgA Abs have remained obscure. Here, we show that neutralizing anti-RBD Abs recognize distinct commensal strains in the human microbiota. Vaccination-induced salivary Abs promoted the expansion of these commensals, and supplementation of vaccinated individuals with one such strain increased the concentrations of anti-SARS-CoV-2 IgG in the oral cavity. Altogether, our data demonstrate a cross-regulation of salivary anti-S Ab responses and distinct bacteria of the nasopharyngeal microbiota.

RESULTS

Oral microbiota changes during vaccination are associated with the induction of salivary Ab responses

Abs that are found at the mucosal surfaces are actively transported from the body through the layer of epithelial cells (ECs). For this transport from the basolateral to the apical side of ECs lining the mucosal tract, ECs express specific receptors, such as the neonatal Fc receptor (FcRn) and the polymeric immunoglobulin receptor (pIgR).[31,32] The pIgR mediates the transport of IgA and is ubiquitously expressed by ECs of the oral and gastrointestinal tract. FcRn mediates the transport of IgG, and in adult humans, it is expressed only by EC of the oral cavity.[31] Accordingly, saliva of healthy individuals contains both IgG and IgA, whereas the luminal content, i.e., feces, of the gut contains IgA but not IgG (Figures 1A–1C). We recruited 19 healthy participants to study the microbiota-Ab interaction during the first month after vaccination. Among them, only one of the participants exhibited anti-nucleocapsid (NCP) IgG in the serum (Figure S1A), whereas the others lacked such Abs, indicating their naive status with regard to SARS-CoV-2 exposure. Next, we quantified the amount of anti-S1 of S IgG and IgA in the oral

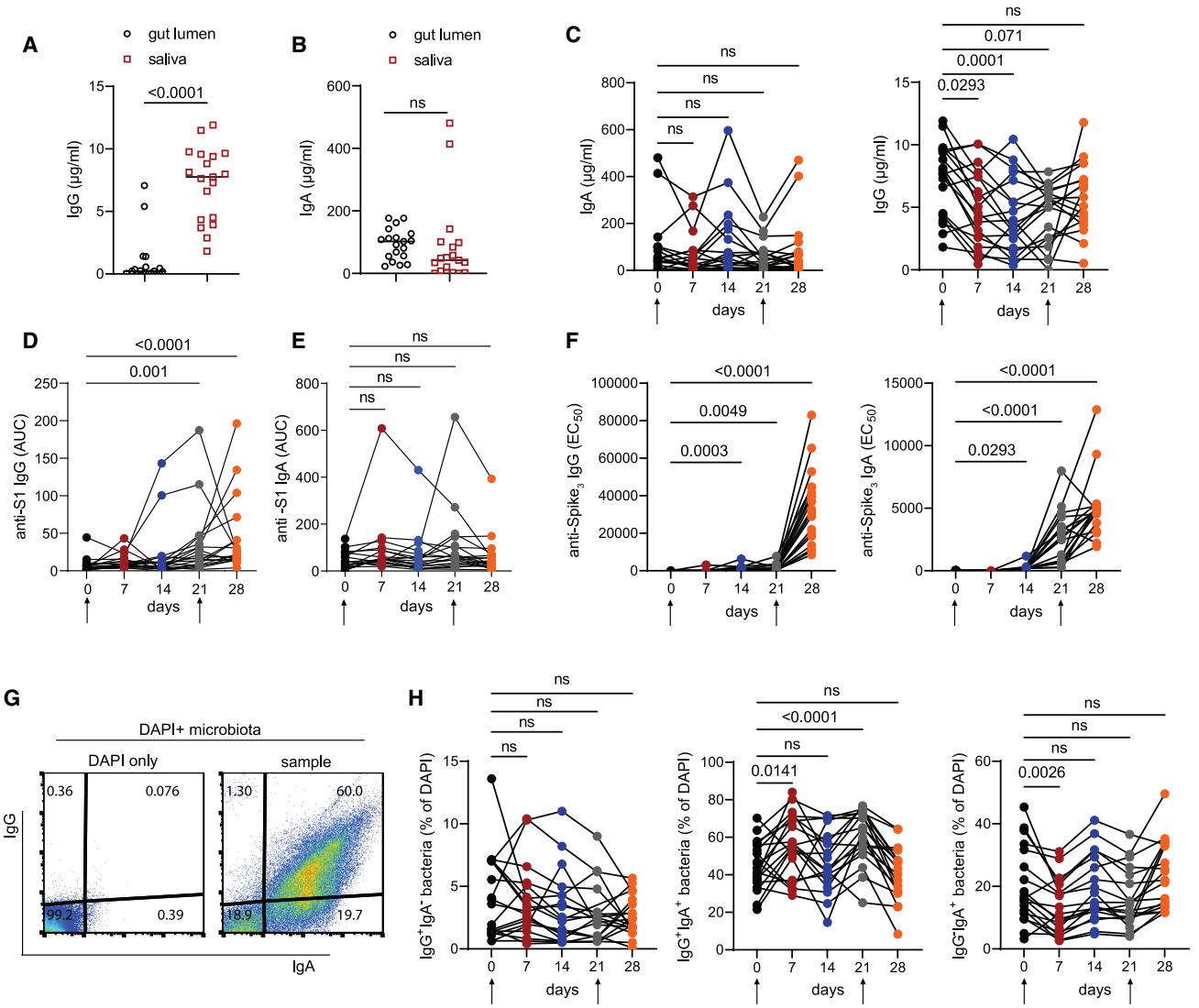

Figure 1. Oral antibody responses during first month of BNT162b2 vaccination

(A and B) Total levels of salivary and fecal IgG (A) and IgA (B) levels in healthy volunteers before vaccination.

(C) Total levels of salivary IgA and IgG levels during BNT162b2 vaccination course.

(D and E) Anti-Spike IgG (D) and IgA (E) levels in the saliva of healthy individuals vaccinated with BNT162b2 vaccine.

(F) Anti-Spike IgA and IgG levels in serum during BNT162b2 vaccination course.

(G) Representative dot plots showing salivary bacteria IgA and IgG coating during the course of BNT162b2 vaccination. Oral microbiota was stained using anti-human IgG and anti-human IgA antibodies and frequencies of IgA/IgG-coated bacteria were determined by flow cytometry.

(H) Frequencies of IgG^+IgA^-, IgG^-IgA^+, and IgG^+IgA^+ bacteria in the saliva during the course of BNT162b2 vaccination. Arrows (at days 0 and 21) indicate days of vaccination.

Each dot represents one participant. Bars (A, B) represent the median. Mann-Whitney test was used in (A) and (B). Friedman test with Dunn's multiple comparisons (C–F and H) was used. $p < 0.05$ were considered statistically significant. Ns, not significant.

cavity during the first month after the primary vaccination against SARS-CoV-2 (Figures 1D and 1E). For 19 healthy participants vaccinated with BNT162b2 (Table S1 for detailed information), high amounts of anti-S1 IgG Abs (in 10 of the 19 participants) were detectable in the saliva at day 21, whereas the other 9 showed only low anti-S1 IgG titers. The Ab response further increased in all participants until day 28, 7 days after administration of the second dose of the vaccine (Figure 1D). That was in line with the induction of serum anti-SARS-CoV-2 S IgG (Figure 1F). No significant induction of anti-S1 or anti-S_3 IgA at the mucosal surfaces was observed, although anti-S1 IgA was present in the serum (Figures 1E, 1F, and S1B). Thus, in agreement with a previous report,[33] vaccination with BNT162b2 induced anti-S IgG Abs in the oral cavity, starting from day 21 after the initial vaccine dose.

Since vaccination induced the secretion of anti-S Abs into the oral cavity, we next evaluated whether the profile of bacterial coating with salivary Abs changes during vaccination. We observed high coating of oral microbiota by secreted IgA and IgG Abs (Figure 1G). Noteworthy, most of the bacteria were

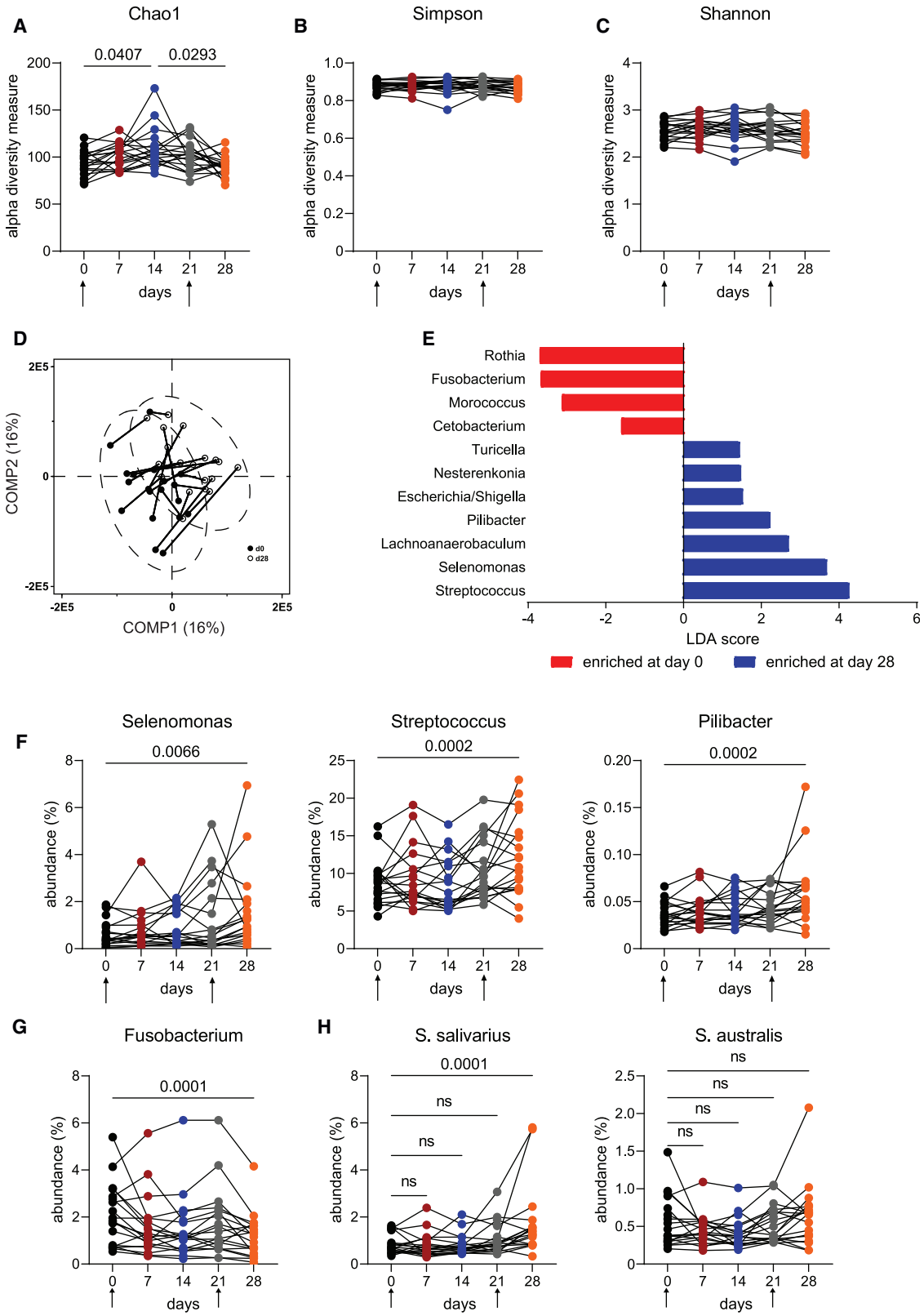

Figure 2. Oral microbiota composition during first month of BNT162b2 vaccination

(A–C) Richness of microbiota composition during the course of BNT162b2 vaccination.

(D) Principal-component analysis (PCA) of salivary microbiota at days 0 and 28 of BNT162b2 vaccination.

(legend continued on next page)

bound by both IgA and IgG Abs (Figures 1G and 1H). Further analysis at various time points after vaccination revealed increased frequencies of IgG^+IgA^+ bacteria in the saliva at day 21 after vaccination, the time point when significant anti-S Ab responses had developed (Figure 1D). To analyze the impact of vaccination-induced anti-S IgG Abs on the bacterial composition, we compared salivary microbiota before and after vaccination in 19 individuals. The overall diversity (Chao1, Simpson, and Shannon indexes) of the oral microbiota did not change following vaccination (Figures 2A–2C). However, the composition of microbiota at day 0 and day 28 after primary dose clustered separately, as revealed by principal-component analysis (PCA) (Figure 2D). Since the salivary microbiota is characterized by not only high inter-individual variability but also high intra-individual stability,[34–36] we checked whether the observed differences were due to the regular fluctuation of microbiota by following oral microbiota composition after vaccination (Figure S2). Changes in the composition of salivary microbiota were observed starting from day 21 after primary vaccination, correlating with the induction of salivary anti-S Ab responses (Figures 1D and S1B), but not before, further suggesting that compositional changes of the oral microbiota can be influenced by anti-S Abs. Subsequent comparison of oral microbiota composition by linear discriminant analyses (LDAs) combined with effect size measurements (LEfSe) at day 0 and day 28 showed that *Streptococcaceae* and *Enterococcaceae* families were enriched in the oral microbiota at day 28, whereas *Micrococcaceae* and *Fusobacteriaceae* family members were reduced, respectively (Figure S2A). At the genus level, LEfSe analysis revealed that at day 28, *Turicella*, *Nesterenkonia*, *Escherichia/Shigella*, *Pillibacter*, *Lachnoanaerobaculum*, *Selemonas*, and *Streptococcus* were enriched at day 28, whereas *Rothia*, *Fusobacterium*, *Morococcus*, and *Cetobacterium* were found to be diminished at day 28 (Figure 2E). When following relative abundances of bacterial genera identified by LEfSe over time after vaccination, we observed an increase of *Selemonas* (in 16 of the 19 participants), *Pillibacter* (in 14 of the 19), and *Streptococcus* (in 14 of the 19: from 8.8% ± 3.0% at day 0 till 12.1% ± 5.3% at day 28) (Figure 2F). A reduction in *Fusobacterium* (in 14 of the 19) occurred only on day 28 after primary vaccination (Figure 2G). Changes in *Rothia* and *Escherichia/Shigella* genera were not statistically significant (Figures S2B and S2C). In view of the high LDA score of *Streptococci* (Figure 2E), further classification of *Streptococcus* genera showed that frequencies of *Streptococcus salivarius*, but not *Streptococcus australius*, were significantly increased in the oral cavity at day 28 after vaccination, in 14 of the 19 participants (means of *S. salivarius* at days 0 and day 28 were 0.8% ± 0.4% and 1.8% ± 1.5%) (Figure 2H). To further verify the increase of *S. salivarius*, we have defined *Streptococci* species during vaccination by minimal entropy decomposition approach.[37] Only oligotypes corresponding to *S. salivarius* were increased during the vaccination course (Figure S3), further suggesting that vaccination correlates with the *S. salivarius* abundance in the oral cavity. Next, we performed correlation analysis of *S. salivarius* abundance with anti-S Ab levels. Although no correlation was observed between *S. salivarius* and virus-neutralizing capacity neither at day 0 nor day 28 (Figures S4A and S4B), levels of this bacteria correlated with the levels of both anti-S1 IgG and anti-S1 IgA (Figures S4C–S4F), suggesting that both neutralizing and non-neutralizing anti-S Abs may have an impact on the enhanced presence of *S. salivarius*.

To further address whether such changes might be attributed to the temporal changes in the microbiota, we have analyzed publicly available datasets evaluating the salivary bacterial composition during 1 month.[38,39] We did not observe any differences in *Streptococcus* abundance in those studies, further indicating that such changes are associated with vaccination (Figure S5A). We have previously reported that rheumatoid arthritis (RA) patients do not develop salivary anti-S Abs during the first month after immunization.[40] Thus, we next analyzed the salivary microbiota in RA patients during vaccination (Figure S5B). Consistent with the lack of salivary anti-S Abs, *Streptococcus* abundance in RA patients did not change during the first 28 days after vaccination (Figure S5B; Table S2). Finally, the *S. salivarius* abundance was similar between healthy individuals at day 28 and subjects from an independent cohort recruited several months after vaccination, suggesting a temporal effect on the *S. salivarius* increase during vaccination (Figure S5C; Table S3). Of note, such temporal oral microbiota fluctuations were not associated with any clinically relevant observations in the participants, despite some reported cases of diarrhea associated with vaccination.[41] Altogether, these data further support a link between oral anti-S Abs and changes in the microbiota composition.

Participants differed in their salivary anti-S1 IgG levels at day 21 after vaccination (Figure 1D), and their salivary Ab response correlated with serum anti-S levels (Figure S6A). We therefore divided them into "high" (anti-S1 IgG: 60.5% ± 55%) and "low" (anti-S1 IgG: 9.0% ± 5.1%) responders in terms of anti-S IgG titers and compared their oral bacterial composition (Figures S6B–S6E). LEfSe analysis between these two subgroups revealed decreased *Olsenella* and *Peptostreptococcaceae_insertae_sedis* and enhanced abundances of *Solobacterium* and *Pseudomonas* in low responders (Figures S6C and S6E). None of these bacterial genera, except *Solobacterium*, were significantly affected during the course of vaccination (Figure S6D). This finding indicates that the observed increase in *Streptococci* during vaccination was not primarily influenced by the levels of salivary anti-S IgG responses but rather associated with the generation and secretion of such Abs.

Since the intestine is an organ densely populated with commensal microbiota,[9] we next analyzed whether vaccination

(E) LDA scores of genera of salivary microbiota at day 0 and at day 28 of BNT162b2 vaccination. Linear discriminant analysis (LDA) combined with effect size measurements (LEfSe) was performed for 16S rRNA datasets obtained from saliva of vaccinated individuals. A p value of <0.05 was considered significant in Kruskal-Wallis test, and respective genera were depicted.

(F and G) Relative abundances of *Selenomonas*, *Fusobacterium*, *Pilibacter*, and *Streptococcus* during BNT162b2 vaccination.

(H) Relative abundancy of *S. salivarius* and *S. australis* in the saliva during BNT162b2 vaccination.

Each dot represents one participant. Friedman test with Dunn's multiple comparisons (A–C and F–H) was used. $p < 0.05$ were considered statistically significant. Ns, not significant.

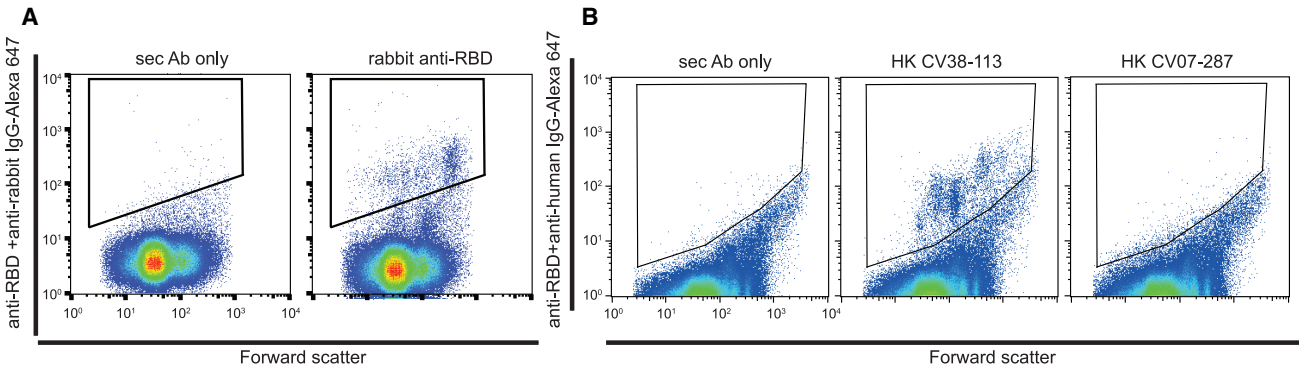

C

clone	HC-001	HC-003	HC-011	HC-009	HC-043
HK CV38-113	0	1,65	0,72	1,14	2,09
HK CV07-287	0	0	0	0	0
HL CV07-270	2,1	6,59	5,46	5,31	5,11
HK CV-X2-106	0	1,06	0	0	0
HK CV07-283	0,74	0,89	0	0	0
HL CV07-262	0,64	0,64	0	0	0
HL CV07-250	0	0	0	0	0
HL CV07-222	0,55	1,37	0	0	0
HK CV-X1-126	1,04	0,86	2,36	1,95	2
HL CV07-200	1,68	1,51	0	0	0,32
HL CV07-315	0,85	1,03	2,14	1,04	1,56
HK CV38-221	1,9	0,86	0	0	2,5
HK CV38-139	1	1,42	2,94	1,75	2,94
HK CV05-163	2,15	5,15	3,46	2,66	1,61
HL CV07-255	1,87	2,76	0	1,28	0,44
rabbit anti-RBD	1,01	3,82	0,17	0,9	0,32

D

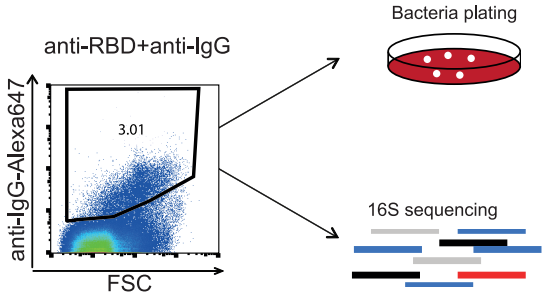

E

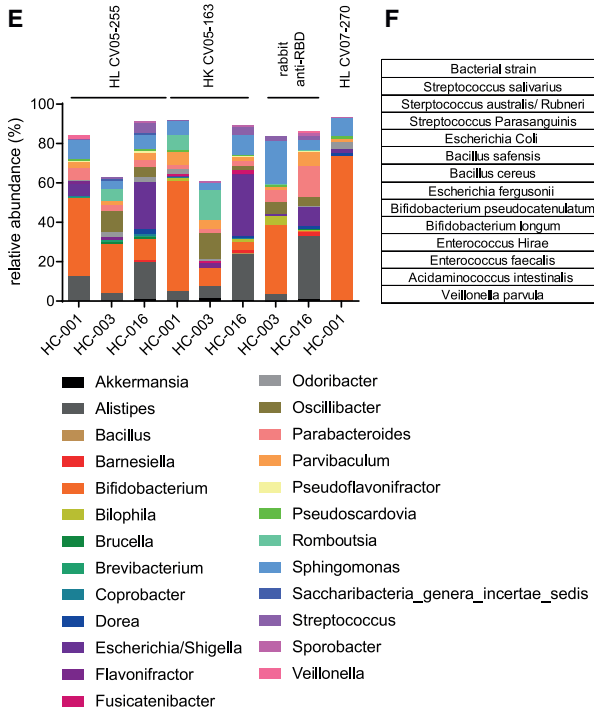

F

Bacterial strain	rabbit anti-RBD	HL CV07-270	HK CV-X1-126	HL CV07-200	HL CV07-315	HK CV05-163	HL CV07-255
Streptococcus salivarius	x	x			x		x
Sterptococcus australis/ Rubneri	x						x
Streptococcus Parasanguinis		x			x		x
Escherichia Coli	x	x			x	x	x
Bacillus safensis	x			x	x		
Bacillus cereus				x	x		
Escherichia fergusonii	x	x			x		
Bifidobacterium pseudocatenulatum		x					x
Bifidobacterium longum							x
Enterococcus Hirae		x					x
Enterococcus faecalis			x		x		
Acidaminococcus intestinalis					x		
Veillonella parvula					x		

Figure 3. Neutralizing anti-RBD antibodies recognize distinct commensal bacteria

(A) Representative dot plots of human fecal microbiota stained with neutralizing anti-RBD antibody raised in rabbit. Left plot shows the binding of secondary anti-rabbit IgG-Alexa 647 antibody.

(B) Representative dot plots of microbiota stained with monoclonal neutralizing anti-RBD antibodies derived from COVID-19 patients (HK CV38-113 and HK CV07-287 clones). Left plot shows the binding of secondary anti-human IgG-Alexa 647 antibody.

(legend continued on next page)

also impacted the fecal microbiota composition throughout the first month after vaccination. We neither observed any significant induction of anti-S-SARS-CoV-2 IgA responses during the 28 days after primary vaccination (Figure S7A), nor changes in microbial diversity (Chao1, Simpson, and Shannon indexes) (Figure S7B; data not shown). Subsequent LEfSe analysis revealed that three bacterial families, *Leptotrichiaceae*, *Xanthomonodaceae*, and *Succinivibrionaceae*, and 5 respective genera, *Sneathia*, *Anaerotruncus*, *Herbaspirillum*, *Succinivibrio*, and *Stenotrophomonas*, were changed in the fecal microbiota between days 0 and 28 after the primary vaccine dose (Figures S7C–S7G). Notably, these bacterial families represent minor (relative abundance less than 0.1%) members of the microbial community of the gut. Thus, vaccination did not detectably affect fecal microbiota composition in the time window studied here. Altogether, the oral, but not fecal, microbiota composition exhibited distinct changes during the first month after the application of the initial dose of the vaccine that was associated with the secretion of anti-S-SARS-CoV-2 IgG Abs into the saliva.

Anti-S Abs recognize various microbial species via molecular mimicry

The temporal microbiota composition in the oral cavity is relatively stable, but it still exhibits some degree of fluctuation over time.[34–36] Given that changes in the composition of salivary microbiota upon vaccination did correlate in time with the induction of anti-S-SARS-CoV-2 Abs, we hypothesized that S specific Abs might bind to distinct commensal bacteria and influence their abundance. To test this hypothesis, we stained the fecal microbiota of healthy, non-vaccinated individuals (Table S4 for detailed information) with neutralizing Abs specific for the RBD of the S protein of SARS-CoV-2 (Figures 3A–3C) that were either generated by immunizing rabbits or were cloned from hospitalized COVID-19 patients.[42] The rabbit Ab and 13 of the 15 human monoclonal neutralizing Abs tested bound to distinct commensal bacteria. The two monoclonal Abs without binding activity were used as isotype controls heavy kappa (HK) CV07-287 and heavy lambda (HL) (CV07-250; Figure 3C). Co-staining of microbiota with rabbit and human monoclonal Abs revealed that different Abs specific for RBD may recognize similar bacteria (Figure S8A), indicating that the bound bacteria may express surface antigens mimicking the RBD of SARS-CoV-2.

To identify the bacterial genera bound by the anti-RBD Abs, we isolated those bacteria by fluorescence-activated cell sorting (FACS) and determined their 16S ribosomal DNA (rDNA) genotype (Figure 3D). Bacteria that had been labeled by the secondary Abs (anti-human IgG and anti-rabbit IgG) were excluded from the analysis (File S1). We could identify several bacterial genera recognized by one or more of the anti-RBD Abs (Figure 3E; File S1). The monoclonal human anti-RBD Abs showed specific reactivity toward *Streptococcus*, *Escherichia*, *Bifidobacteria*, and others (Figure 3E). Genera identified differed among various donors (Figure 3E), highlighting the inter-individual diversity of the microbiota and showing that the anti-RBD Abs tested could bind to several distinct bacterial genera. The binding of the anti-RBD IgG Abs to the microbiota was distinct, as far as it differed from that of the secondary anti-IgG Abs used (File S1), and from the binding pattern of a non-autoreactive, non-RBD specific human HK mGO53 IgG Ab[43] (Figure S8B; File S1). In addition to that, 3 S (non-S1) binding, non-neutralizing Abs (HL CV03-163, HL CV03-177, and HL CV05-115) were analyzed for their reactivity to the microbiota. Only HL CV03-177 showed binding to the microbiota (Figures S9A and S9B). Further 16S sequencing revealed the distinct, non-overlapping pattern of bacteria identified by neutralizing, RBD-specific Abs (File S1). To further analyze the non-specific binding of Abs, we have selected clonally related anti-RBD Abs that differed only by one amino acid in their heavy-chain complementarity-determining region 3 (CDRH3) region (Figure S10A) and analyzed their binding to the microbiota. Single amino acid substitution of CDRH3 affected the binding to microbiota, further arguing for specific recognition of at least cloned bacterial strains (Figure S10B). We concluded that neutralizing anti-RBD Abs can bind to distinct bacterial species of the microbiome.

To identify the bacterial molecular mimics recognized by the anti-RBD Abs, we isolated bacteria binding to such Abs from the fecal microbiota of eight healthy donors by FACS and cultivated them in selective bacterial media under anaerobic culture conditions. Individual bacterial colonies were identified according to their 16S rDNA sequences (Figures 3D and 3F). Consistently with 16S sequencing data (Figure 3E; File S1), two *Bacilli* species, three *Streptococcus* species, two *Bifidobacterium* species, two *Enterococcus* species, as well as *Veillonella parvula* and *Acidaminococcus intestinalis* were identified (Figure 3F). Staining of cultured bacteria confirmed their recognition by anti-RBD Abs (Figures S11A and S11B). Interestingly, *S. salivarius* that was found to be increased in the oral cavity of vaccinated humans was recognized by three of the monoclonal Abs tested and the rabbit anti-RBD Abs (Figures 3F and S10C). A probiotic strain of *S. salivarius K12 (Bactoblis)*, was also recognized by the rabbit anti-RBD Abs (Figure S11A). Of note, some bacterial cultures showed only partial staining with anti-RBD Abs, probably reflecting the heterogeneity of bacteria during growth or community-dependent variability in gene expression (Figure S11).

Induction of cross-reactive anti-S Abs by commensal microbiota strains

Having identified distinct bacterial mimics of RBD, we next investigated whether the bacteria expressing these proteins

(C) Frequencies of bacteria bound by human neutralizing anti-RBD antibodies and one derived from rabbit toward microbiota from healthy individuals. Fecal microbiota from 5 healthy donors were stained with 15 monoclonal anti-RBD antibodies from COVID-19 patients or anti-rabbit RBD, followed by respective secondary fluorochrome-coupled antibodies. Bound bacterial fraction was defined via comparison of stained sample with sample stained only with secondary antibody.

(D) Strategy for the identification of bacteria that are bound by anti-RBD antibodies.

(E) Relative abundance of selected bacterial genera in sorted bacterial fractions from healthy individuals (HC) bound by respective anti-RBD antibodies. 16S rRNA V3-V4 region of sorted bacteria was sequenced and annotated to corresponding bacteria. Abundance was calculated in relation to the number of total reads. Genera with abundance higher than 0.1% were further selected.

(F) List of cloned bacteria isolated based on the binding to anti-RBD antibodies.

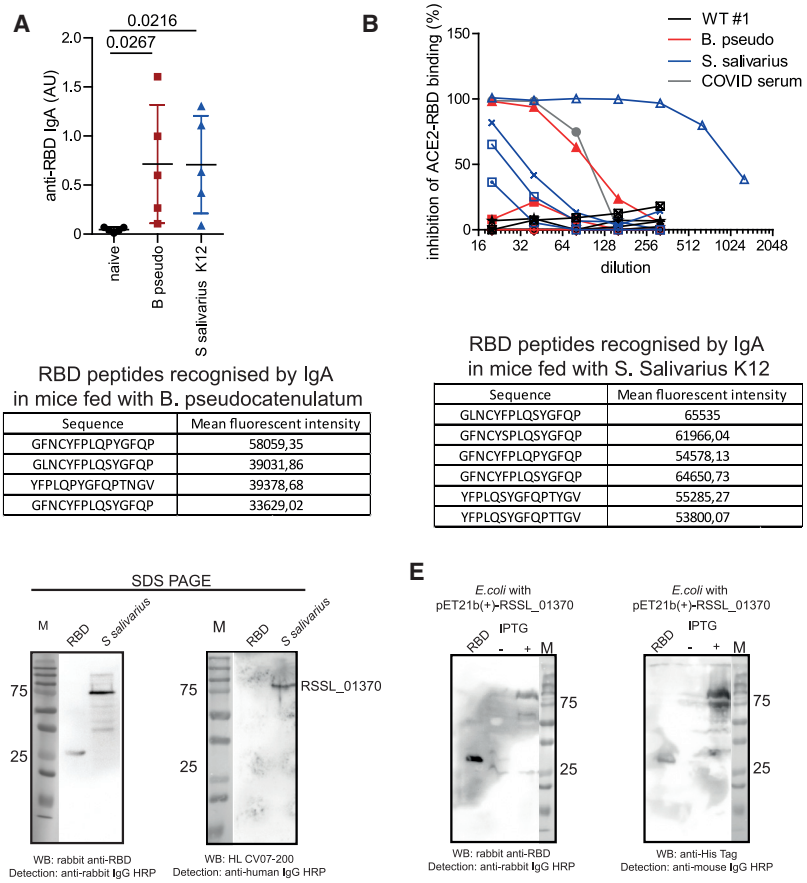

Figure 4. Induction of cross-reactive anti-RBD SARS-CoV-2 response by commensal bacteria

(A) Induction of anti-RBD IgA response by oral bacterial supplementation. Mice were orally gavaged every second day as described in STAR Methods. Anti-RBD IgA was analyzed in fecal supernatants.

(B) Inhibition of ACE2-RBD by fecal supernatants from mice treated as in (A).

(C) RBD peptides recognized by the antibodies elicited upon oral supplementation of mice with *S. salivarius K12* and *B. pseudocatenulatum* for 3 weeks. Anti-RBD IgG titers at day 14 in mice immunized with heat-killed *S. salivarius* and *B. pseudocatenulatum*. Mice were immunized as described in STAR Methods.

(D) Western blot analysis of rabbit anti-RBD and HL CV07-200 binding to *S. salivarius* lysate isolated from human microbiota. Recombinant SARS-CoV-2 RBD-His-Tag (left lane) was used as positive control.

(E) Western blot analysis of rabbit anti-RBD to RSSL-01370 expressed in *E. coli*. Recombinant SARS-CoV-2 RBD-His-Tag (left lane) was used as positive control. Data in (A) are shown as mean ± SD. Each line in B represents one animal. Kruskal-Wallis test with Dunn's multiple comparisons was used for (A). $p < 0.05$ were considered statistically significant. Ns, not significant.

could induce a cross-reactive anti-RBD Ab response *in vivo*. We focused on *S. salivarius* and *B. pseudocatenulatum*, taking into account that *S. salivarius* is increased in humans after the first month upon vaccination (Figure 2H) and on *B. pseudocatenulatum* abundance which inversely correlates with the development of the post-COVID-19 acute syndrome.[44] Considering that these bacteria can be normal constituents of the microbiota, we fed C57BL/6 mice by oral gavage with *S. salivarius K12* or *B. pseudocatenulatum* to test whether a cross-reactive IgA response would be induced. Within 21 days, fecal IgA reactive to RBD was detectable in mice fed with both *S. salivarius K12* and *B. pseudocatenulatum* (Figure 4A). Fecal supernatants also inhibited binding of RBD to ACE2, indicating that those RBD Abs had neutralizing capacity (Figure 4B).

We next mapped the epitopes of the S SARS-CoV-2 protein, recognized by the IgA Abs that were induced by oral supplementation of mice with the bacteria. Of the 564 peptides representing the S protein of SARS-CoV-2, IgA induced by both *B. pseudocatenulatum* and *S. salivarius K12* recognized the peptide sequence GFNCYFPLQSYGFQPTNGV (Figures 4C and S12A). Indeed, the peptide recognition motifs of rabbit anti-RBD and human HL CV07-200 anti-RBD Abs included this sequence in their receptor-binding motif (RBM) epitope (Figures S12B–S12D). This peptide corresponds to the RBM of RBD, in line with the ACE2-RBD inhibition data (Figure 4B), and has homology to reference standard sequence library (RSSL)-01370 of *S. salivarius K12* (Figures S12E–S12G). These data show that oral supplementation of mice with *S. salivarius K12* and *B. pseudocatenulatum* can induce Abs cross-reactive to the RBM of the S protein of SARS-CoV-2 in mice *in vivo*.

Western blot analysis of bacterial lysates revealed that rabbit anti-RBD Abs and the human anti-RBD IgG Ab HL CV07-200 recognize discrete proteins of *S. salivarius* and *B. pseudocatenulatum* (Figures 4D and S13A–S13C). We identified the *S. salivarius* protein by mass-spectrometry as the uncharacterized protein RSSL-01370, putative dextransucrase (Table S5).[45] We confirmed the binding of RSSL-01370 from *S. salivarius K12* to anti-RBD Abs, by cloning the encoding gene in *E. coli* and detecting this recombinant protein with the anti-RBD Abs (Figure 4E). Taken together, these data demonstrate that distinct commensal microbiota expresses proteins that selectively mimic RBD and that are recognized by neutralizing anti-RBD Abs.

To further show that RSSL-01370 can induce anti-RBD Abs, mice were immunized with purified RSSL-01370. Consistently, RSSL-01370 immunization induced anti-RBD and anti-S1 IgG Abs in the serum, indicating that this bacterial protein can induce cross-reactive Abs against the S of SARS-CoV-2 (Figure 5A). Further cloning of Abs from RSSL-01370 immunized mice revealed the presence of Abs that neutralize S-pseudotyped lentivirus entry into ACE2-expressing 293 T cells, albeit at higher concentrations than Abs isolated from COVID-19 patients (Figures 5B and S14). Thus, RSSL-01370 protein from *S. salivarius* can induce neutralizing anti-S Abs.

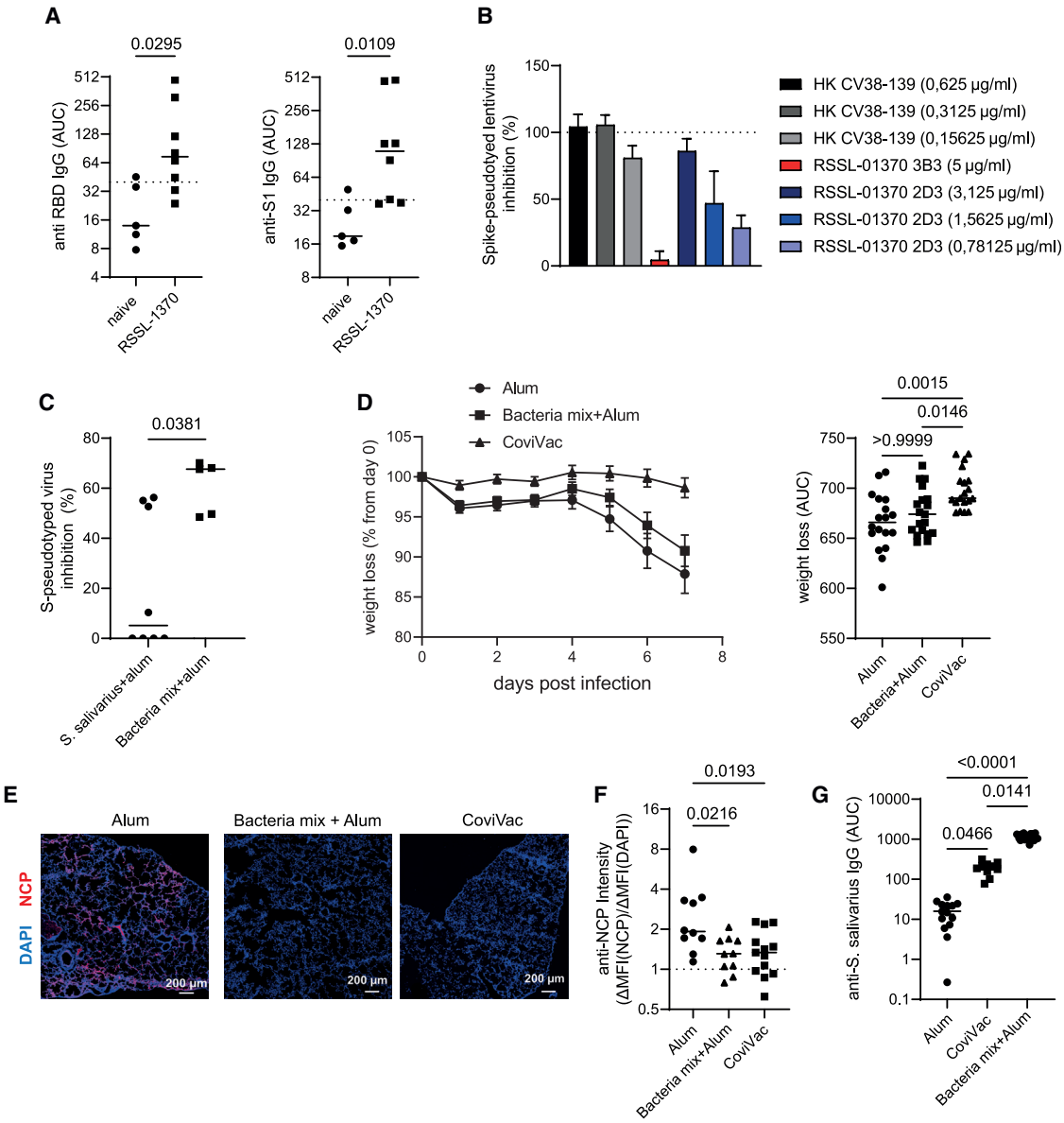

Figure 5. Inhibition of SARS-CoV-2 infection by cross-reactive anti-Spike antibodies elicited by commensal bacteria

(A) Sera anti-RBD and anti-S1 IgG levels in mice immunized with purified RSSL-01370 protein.

(B) Inhibition of S-pseudotyped lentivirus entry to ACE2 expressing 293 T cells by monoclonal antibodies.

(C) Inhibition of S-pseudotyped lentivirus entry to ACE2 expressing 293 T cells by serum from mice immunized either with *S. salivarius* or *S. salivarius*/*B. pseudocanulatum*/*B. longum*.

(D) Weight loss of K18-hACE2 Tg mice immunized either with bacteria or with CoviVac (at days 0 and 14) and infected with 10^4 TCID B1.1 SARS-CoV-2 (day 21).

(E) NCP protein staining of lung from B1.1 SARS-CoV-2 infected K18-hACE2 Tg mice at day 7 post-infection. Scale bar represents 200 µm.

(F) Intensity of NCP protein staining in the lungs of B1.1 SARS-CoV-2 infected K18-hACE2 Tg mice at day 7 post infection.

(G) Sera anti-*S. salivarius* IgG levels in mice immunized with bacteria or with CoviVac. Data in (B) and (D) are shown as mean ± SD, in (A), (C), (D), (F), and (G) as individual dots and median. Mann-Whitney test was used in (A) and (C). Kruskal-Wallis test with Dunn's multiple comparisons was used for (D), (F), and (G). $p < 0.05$ were considered statistically significant. ns, not significant.

To further test the *in vivo* relevance of bacteria-induced Ab responses on viral clearance, we immunized C57BL/6 mice either with *S. salivarius K12* alone or in combination with *B. pseudocatenulatum* and *B. longum*. We noted that mice vaccinated with the bacterial mixture showed a higher capability to inhibit infection of ACE2-293 T cells with S-pseudotyped virus (Figure 5C). Thus, we next immunized K18-hACE2 Tg mice with the bacterial mixture and infected them with 10^4 tissue-culture infectious dose (TCID) B1.1 SARS-CoV-2 intranasally 3 weeks later. Mice immunized with whole-virion inactivated SARS-CoV-2 (CoviVac) emulsified in alum were used as control.[46] Although bacteria-treated mice did not show any significant

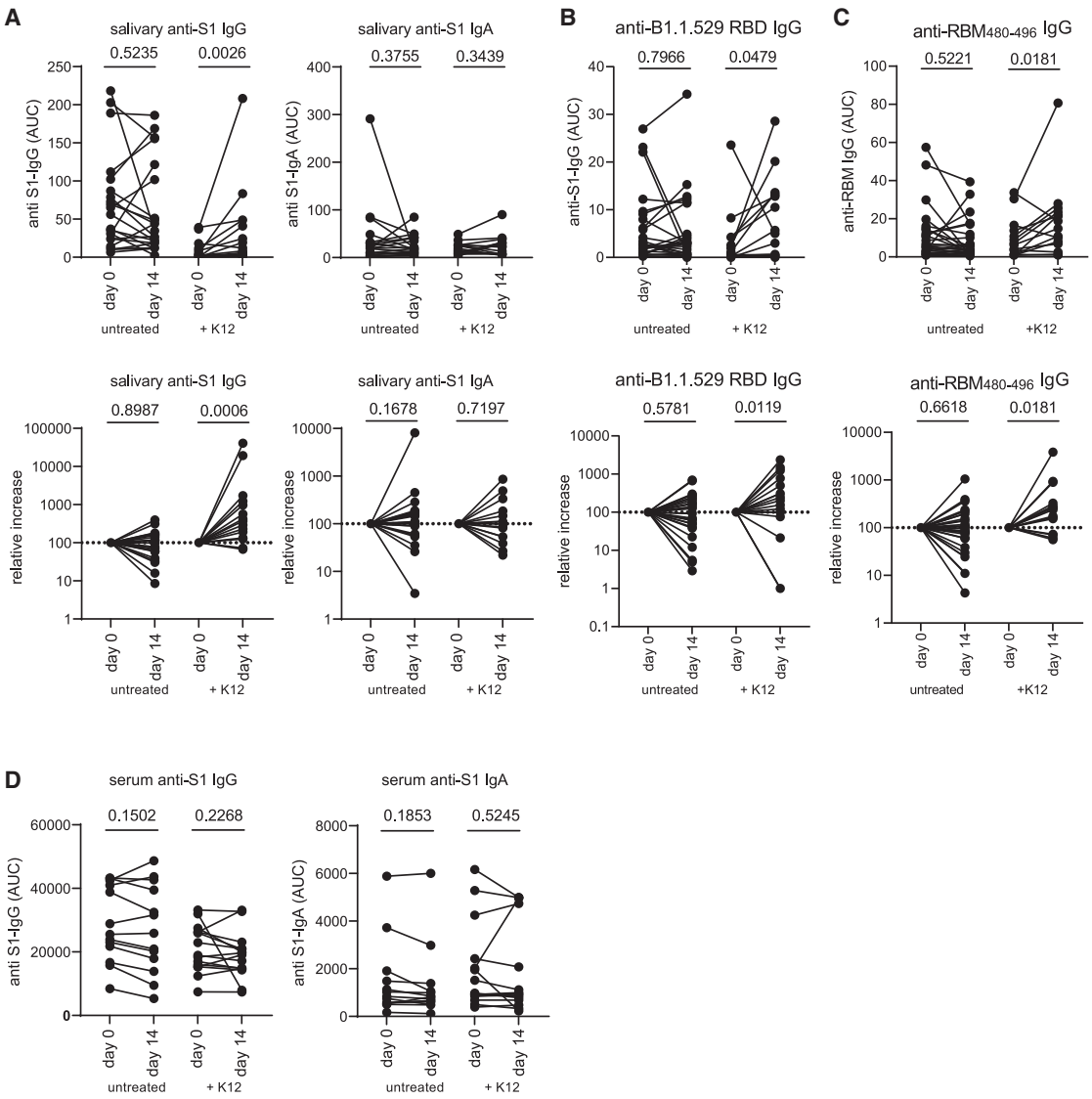

Figure 6. Induction of cross-reactive anti-RBD SARS-CoV-2 response by *Streptococcus salivarius K12* in vaccinated humans

(A) Absolute values (top) and relative increase (bottom) of salivary anti-S1 IgG and IgA levels after oral *S. salivarius K12* supplementation for 2 weeks. Area under the curve (AUC) was calculated for each sample. Relative increase was calculated as following: AUC(day 14)/AUC(day 0)*100.

(B and C) Absolute values (top) and relative increase (bottom) of salivary anti-B1.1.529 RBD IgG (B) and anti-$RBM_{480–496}$ (C) IgG by oral *S. salivarius K12* supplementation for 2 weeks. Binding was assessed by ELISA using serial dilutions of saliva. Area under the curve (AUC) was calculated for each sample. Relative increase was calculated by the following formula: relative increase = AUC(day 14)/AUC(day 0) * 100.

(D) Serum anti-S1 IgG and IgA levels after oral *S. salivarius K12* supplementation for 2 weeks. Each dot represents one participant. Wilcoxon matched-pairs signed rank test was used for (A)–(D). $p < 0.05$ were considered statistically significant. ns, not significant.

amelioration of overall disease (Figure 5D), virus clearance from the lungs was accelerated (Figures 5E and 5F), suggesting that cross-reactive Abs contribute to the viral clearance *in vivo*. Finally, mice immunized with CoviVac also produced IgG Abs reacting to *S. salivarius* (Figure 5G), further highlighting the cross-reactivity between anti-viral immune responses and certain bacterial strains.

We next analyzed whether oral supplementation of humans with the probiotic *S. salivarius K12* affects the nasopharyngeal S-specific Ab levels in vaccinated individuals. To this end, fully vaccinated individuals who had their last vaccination at least 3 months prior to enrollment in this study were supplemented orally with 10^7 colony-forming unit (CFU) of *S. salivarius K12* daily for 2 weeks (Table S6 for detailed information on the cohort). Their salivary and serum anti-S Ab levels were compared before supplementation and 2 weeks later. Within 2 weeks, *S. salivarius K12* supplementation induced a significant increase in anti-S1 IgG responses in the saliva of 13 of the 19 probands (day 0: 8.5 ± 12.1 vs. day 14: 28.5 ± 48.8), an increase that was not observed in the control group (Figure 6A). Importantly, we also observed increased reactivity toward the RBD of the Omicron/B1.1.529 variant of SARS-CoV-2 (day 0: 2.8 ± 5.8 vs.

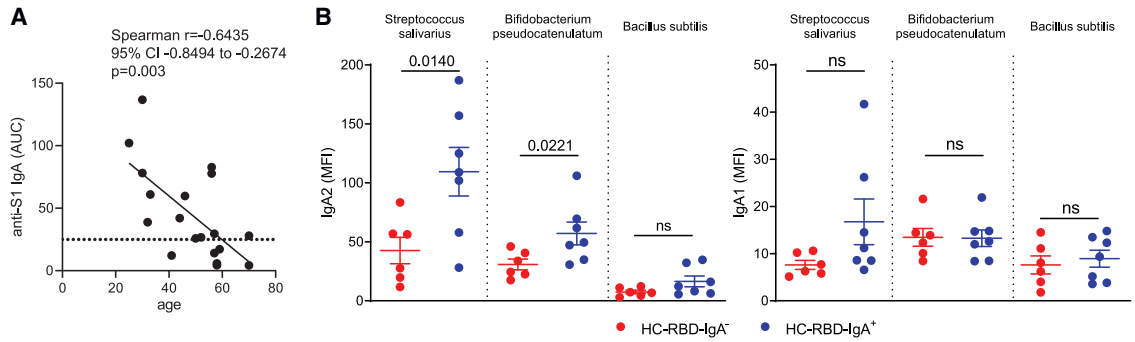

Figure 7. Cross-reactive anti-RBD IgA antibodies in non-vaccinated individuals recognize commensal bacteria

(A) Correlation of the levels of salivary anti-S1 IgA with the age in healthy individuals.

(B) Mean fluorescent intensity of IgA1 and IgA2 coating of various bacterial strains using saliva from donors who had anti-RBD IgA (HC-RBD-IgA$^+$) and those who did not (HC-RBD-IgA$^-$) in their saliva. Spearman correlation was quantified in (A). Unpaired t test was used for (B). Each dot represents one participant. $p < 0.05$ were considered statistically significant. ns, not significant.

day 14: 6.7 ± 8.5) (Figure 6B). Consistent with the homology between RSSL-01370 and the $RBM_{480–496}$ peptide (Figure S12E), *S. salivarius K12* supplementation also increased titers of salivary IgG Abs against $RBM_{480–496}$ (day 0: 9.0 ± 10.37 vs. day 14: 17.6 ± 18.4) (Figure 6C). Eight of the 19 K12-treated participants also exhibited an increase in salivary S1-specific IgA (day 0: 17.6 ± 13.2 vs. day 14: 26.4 ± 23.2), but the difference did not reach statistical significance (Figure 6A). Serum anti-S IgG and IgA titers were also not significantly affected by K12 supplementation (Figure 6D). These data indicate that oral supplementation with *S. salivarius K12* can stabilize and increase the concentration of S-specific IgG Abs in the oral cavity of BNT162b2 vaccinated humans within 2 weeks.

Since *S. salivarius* is a commensal bacterium that colonizes the oral cavity and may induce local IgA responses there by itself, we next assessed the relation of cross-reactive RBD-specific IgA Abs and the age in the saliva of healthy individuals before vaccination (Table S1; participants at day 0 of vaccination study) and found that the magnitude of the S1-binding IgA responses in the saliva negatively correlated with the age of the donors (Figure 7A). We then addressed whether salivary IgA Abs cross-reacting to RBD would also recognize *S. salivarius* in unvaccinated individuals (Table S7). For this, *S. salivarius*, *B. pseudocatenulatum*, and *B. subtilis* were incubated with saliva from unexposed, unvaccinated humans who exhibited RBD-reactive IgA (healthy controls [HC]-RBD-IgA). We found that the saliva from HC-RBD-IgA positive, but not from negative, individuals contained IgA2 recognizing *S. salivarius* and *B. pseudocatenulatum* (Figure 7B). These data show that RBD-reactive IgA2 can be induced by these bacteria in unexposed, unvaccinated individuals.

To address whether RBD-reactive IgA can be modulated in unvaccinated humans, we supplemented unvaccinated humans with probiotic *S. salivarius K12* (Figures S15A–S15D). In this setting, 2 weeks of supplementation did not induce any significant anti-S1 IgA salivary Ab responses. In addition, anti-S1 IgG was not detected in these participants, consistent with their vaccination status (Figure S15A; data not shown). Further analysis of the oral microbiota composition showed that *S. salivarius K12* reduced the abundance of *Actinomyces* and *Selemonas* genera when compared with individuals of an untreated group (Figures S15A–S15D). Thus, *S. salivarius K12* supplementation affected the levels of anti-S IgG only in vaccinated individuals (Figure 6).

DISCUSSION

The microbiota composition influences the efficiency of vaccination via innate sensing of microbiota by pattern recognition receptors, modulation of antigen presentation by antigen-presenting cells, immunomodulatory effects of bacterial metabolites, and cross-reactive T and B cell responses.[47] In particular, the nasopharyngeal microbiota may contribute to the protection of the host from infection with pathogenic airborne viruses, here SARS-CoV-2, via modulating the ACE2 receptor expression,[48] induction of tonic type I IFN responses,[49] and via tuning of systemic and mucosal transforming growth factor (TGF)-β1 levels, with TGF-β1 controlling Ab class switch recombination to IgA1 and IgA2.[50,51] It is also evident that bacteria of the microbiota provide a vast repertoire of potential molecular mimics for the mucosal immune system, which may provide cross-reactive, pre-existing mucosal immunity against pathogens. Thus, commensal bacteria may contribute to the highly variable susceptibility of humans toward infection with the pathogen. Here, we show that, on one hand, BNT162b2 vaccination supports the persistence of the commensal *S. salivarius* in the oral cavity, and on the other hand, oral supplementation of *S. salivarius* enhanced anti-S Abs in the oral cavity. Such interaction between vaccine-induced Abs and commensal bacterium occurs via molecular mimicry between S protein and RSSL-01370 protein of *S. salivarius* and thereby may provide a further line of protection upon SARS-CoV-2 infection. Thus, we describe the mutual regulation of anti-viral Ab responses and commensal microbiota via molecular mimicry in the context of SARS-CoV-2.

Ab-microbiota interactions at the mucosal surfaces may either result in the depletion of targeted bacteria[18] or in facilitating their persistence.[52] Here, we observe that a SARS-CoV-2 S-expressing vaccine induces salivary Abs correlating with the expansion of certain strains of *Streptococci*, including *S. salivarius*, in line with the notion that vaccine-triggered Abs may help these commensals to persist in the oral cavity. Interestingly, although monoclonal anti-RBD Abs showed quite broad binding toward intestinal microbiota (Figure 3E),

vaccination-elicited salivary Abs did not induce significant changes in the composition of the oral microbiota but rather promoted the growth of beneficial probiotic bacteria. This work reveals the existence of such cross-reactive Abs against both the RBD of SARS-CoV-2 S protein and distinct bacterial peptide mimics, including those of *S. salivarius* and *B. pseudocatenulatum*. Additional oral supplementation of vaccinated people with the probiotic *S. salivarius K12* also enhanced the levels of anti-S Abs in the oral cavity. Altogether, these data demonstrate antigen-specific interactions of commensal bacteria and salivary Abs, and in the case of *S. salivarius* and RBD-specific, cross-reactive Abs, a positive regulatory feedback loop. A limitation of this study is the short period of analysis after vaccination and the small cohort size. Additional studies with longer observation periods and more participants are needed to determine the persistence of this microbiota-Ab crosstalk in the long run.

Bacterial mimics of SARS-CoV-2 S RBD, enhancing a neutralizing mucosal Ab response, are supported by similar observations reported earlier for the HIV-1 virus. In that case, gp41- and gp120-reactive Abs showed cross-reactivity against distinct mimics of microbiota.[24,25,53] In contrast to the SARS-CoV-2 S protein, microbiota-induced gp41-reactive Abs diverted the Ab response generated by Env vaccination from neutralizing to non-neutralizing epitopes on HIV-1 Env.[25] Thus, it will be important to understand why microbial mimics support or deviate protective immune responses.

In case of the SARS-CoV-2 S protein, we observed a positive correlation of certain bacteria with preexisting anti-RBD IgA Abs in healthy, unexposed subjects, and oral supplementation with *S. salivarius* and *B. pseudocatenulatum* induced such cross-reactive Abs in mice. Such preexisting IgA Abs can be explained by the previous exposure of related coronaviruses in humans or the presence of certain bacteria strains in humans, but not in mice. 16S rRNA sequencing of C57BL/6 fecal microbiota further supported the lack of *S. salivarius* and *Bifidobacteria* in these mice (data not shown) and further introduction of these bacteria elicited intestinal IgA response in mice. At the same time, both vaccinated and non-vaccinated did not show further amplification of IgA response (Figures 7 and S15). Further suggesting that *de novo* induction of RBD-reactive IgA and increase in RBD-specific IgG may occur by the colonization of the bacteria, but the contribution of related coronaviruses in the induction of cross-reactive IgAs cannot be excluded at this point. Further experiments are needed to address this question in detail.

Since the pre-existing, cross-reactive Abs are found only in the salivary and intestinal mucosa, but not in the blood, it is unlikely that systemic immune reactions are induced or that the trans-epithelial transport of systemic Abs is significantly affected. Indeed, our analysis of total Ig levels did not reveal any significant changes upon *S. salivarius K12* administration (data not shown). It appears to be a flexible reaction of the local mucosal immune cells, including the induction of short-lived plasma cells. Interestingly, introduction of K12 into mice induced anti-S responses, whereas K12 administration in humans, who harbor *S. salivarius* as commensal, did not significantly increase S-specific IgA in the saliva. By contrast, vaccinated persons supplemented with *S. salivarius* showed the enhanced presence of salivary anti-S1 IgG Abs. Whether these IgG Abs are produced by sort-or long-lived plasma cells, and whether in this case trans-epithelial transport is affected, remains to be shown. Considering that such an increase has been observed not only for wild-type (WT) S but also for omicron RBD and sequence-related RBD of human coronavirus HKU1, but not for sequence-unrelated NL63 RBD (Figure 6; data not shown), it is conceivable that the induction of such Abs may happen locally at the mucosal surfaces via low-affinity interactions. Thus, it would be interesting to evaluate in the future the secreted and systemic Ab repertoire that can be shaped via molecular mimicry. To what extent these modulations of neutralizing salivary anti-RBD Ab concentrations protect from infection and disease remains to be shown. We have found that RSSL-01370 of *S. salivarius* can induce both non-neutralizing and neutralizing Abs against S and subsequently promote viral clearance *in vivo* in an animal model. Two additional studies addressed the impact of *S. salivarius* K12 on COVID-19. In one study, K12 supplementation reduced the incidence of COVID-19 in children during 30 days of K12 supplementation.[54] Another study observed an amelioration of severe COVID-19 in patients treated with *S. salivarius* K12.[55] Thus, *S. salivarius* K12 may promote viral clearance, but larger clinical studies are required in order to provide more substantial evidence for this.

Apart from host-intrinsic factors, the initial virus load may affect disease outcome and severity,[56,57] and there is increasing evidence of microbiota changes during severe COVID-19,[58,59] suggesting that the microbiota composition may be a risk factor for the development of severe disease as well.[58–60] The data are conflicting in terms of the genera associated with disease severity, which is probably due to the heterogeneity of the patient cohorts and differences in treatment. A common denominator is that acute COVID-19 is associated with the prevalence of opportunistic bacteria and depletion of immunomodulatory bacteria.[59] For instance, a distinct oropharyngeal microbiota composition in the COVID-19 patients, characterized by enrichment of opportunistic pathogens such as *Veillonella* and *Megasphaera* and depletion of *Pseudopropionibacterium*, *Rothia*, and *Streptococcus*[61] as well as increased ratios of *Klebsiella*, *Acinetobacter*, and *Serratia* correlate with disease severity.[61] Another study revealed that several *Streptococci* species were depleted in patients with severe disease, which was characterized by high levels of *Mycoplasma salivarium* and lower anti-S IgG levels in the bronchoalveolar lavage fluid.[62] Further comparison of oral microbiota during COVID-19 in unvaccinated and vaccinated individuals showed enrichment of opportunistic bacterial species, including *S. pneumoniae* and *E. coli* in unvaccinated patients, whereas vaccinated individuals showed enhanced the presence of *S. salivarius* and fewer opportunistic species.[63] Finally, a longitudinal assessment of the oral microbiota composition after COVID-19 infection revealed that *Streptococcus* disappeared initially during COVID-19 infection but again reappeared after 1 year.[64] Our data on the salivary microbiota during COVID-19 confirm the depletion of *Streptococcus* during severe COVID-19 (Figure S16; Table S8). Altogether, these data suggest that both viral and microbiota composition may fuel severity of COVID-19.

Earlier reports have described generic fecal microbiota signatures associated with the development of high anti-S Ab titers upon vaccination and with *S. salivarius* being described as positively impacting the titers of neutralizing Abs in the blood of

individuals with a high body-mass index.[65] The presence of other bacteria was reported to correlate with the levels of systemic Ab titers induced by vaccination.[65] The mechanisms of action have been obscure. Here, we demonstrate that distinct bacteria, such as *S. salivarius*, impact on the local presence of SARS-CoV-2-specific Abs in the oral cavity selectively, by the expression of molecular mimics of the RBD of the SARS-CoV-2 S protein. Since we have not seen changes in the general composition of fecal microbiota upon vaccination, those changes in bacterial composition identified by Ng and colleagues most likely function in a so far not deciphered, generic way.[65] Another study also revealed vaccination-induced changes of the oral microbiome.[66] Unfortunately, however, S-specific Ab responses were not analyzed in that study, and the mechanisms involved remained obscure.

In summary, we here provide the first evidence that distinct bacteria of the microbiota of the oro-nasopharyngeal tract contribute to the regulation of mucosal immunity to SARS-CoV-2 by means of their molecular mimicry of the RBD of the SARS-CoV-2 S protein and that they support the persistence of salivary immunity.

STAR★METHODS

Detailed methods are provided in the online version of this paper and include the following:

- KEY RESOURCES TABLE
- RESOURCE AVAILABILITY
  - Lead contact
  - Materials availability
  - Data and code availability
- EXPERIMENTAL MODEL AND STUDY PARTICIPANT DETAILS
  - Human Donors
  - Supplementation of healthy individuals with probiotic bacteria
  - Mice
  - Mice immunizations
  - Mice vaccination and infection
  - Bacteria culture
- METHOD DETAILS
  - Swabs and saliva sample preparation
  - Stool sample preparation from BNT162b2 vaccinated individuals
  - Stool sample preparation for bacteria isolation
  - 16S rRNA gene sequencing and analysis
  - Microbiota staining
  - Microbiota Flow Cytometry
  - Sequencing from bacterial colonies
  - Enzyme-linked immunosorbent assay
  - Analysis of anti-Spike antibody responses by enzyme-linked immunosorbent assay
  - Flow cytometric assay for analysis of antibody responses against Spike protein
  - Epitope mapping for anti-RBD antibodies
  - Inhibition of ACE2-RBD interaction
  - Generation of Spike SARS-CoV-2 pseudotyped lentivirus
  - Inhibition of lentivirus
  - Lung histology
  - Hybridoma generation
  - Protein gel electrophoresis and Western blotting
  - Mass-spectroscopy analysis of proteins
  - Protein expression
  - Protein purification
- QUANTIFICATION AND STATISTICAL ANALYSIS
- ADDITIONAL RESOURCES

SUPPLEMENTAL INFORMATION

Supplemental information can be found online at https://doi.org/10.1016/j.chom.2023.10.007.

ACKNOWLEDGMENTS

We would like to thank Ugur Sahin and Özlem Türeci (Biontech) for the setup of the vaccination clinical study. We are grateful to Timo Rückert, Mona Massoud, Lennard Ostendorf, and Marie Burns for the help in blood collection, to the members of the German Rheumatism Research Center Flow Cytometry Core Facility (T. Kaiser, J. Kirsch, and R. Maier) for help with FACS analysis and cell sorting and to Dr. Mairi McGrath for her careful text editing. We are grateful to Dr. D. Mazurov and Dr. N. Kruglova for sharing the reagents and R. Zvartsev for mice genotyping. Work was supported by DFG (TRR241/B03 and TRR130 P16 to H.-D.C., A.R., and Clinical Research Unit KFO 5023 "BecauseY" Project number 504745852 to A.A.K.; TR-SFB241/A01 (375876048), SFB1444/P11(427826188), SPP1937-DI764/9-2 to A.D.), Dr. Rolf M. Schwiete Foundation (J.N., L.B., and H.-D.C.) and Russian Science Foundation grants # 21-14-00223 (analysis of mucosal antibody responses, to A.A.K.) and Russian Fund for Basic Research #17-00-00435 (V.M.G.) and #17-00-00268 (A.A.K.), by grants from the Leibniz Association (Leibniz Collaborative Excellence, TargArt [M.-F.M.] and ImpACt [M.-F.M. and A.A.K.]), the Berlin Institute of Health (BIH) with the Starting Grant-Multi-Omics Characterization of SARS-CoV-2 infection, Project 6, Identifying Immunological Targets in COVID-19, the state of Berlin and the European Regional Development Fund (ERDF 2014–2021, EFRE 1.8/11, Deutsches Rheuma-Forschungszentrum), and the German Federal Ministry of Education and Research (CONAN and TReAT to M.-F.M. and COVIM P4 to A.D.), by the European Research Council through the Advanced Grants IMMEMO (ERC-2010-AdG.20100317 IMMEMO Grant 268978) to A.R. and ILCAdapt (ERC-2021-AdG 101055309) to A.D., by European Union (GlycanTrigger, 101093997 to A.D.); the Einstein Foundation Berlin (Einstein Professorship to A.D.). J.K., S.M.R., and E.S. are enrolled in the Charité Clinician Scientist Program funded by the Charité-Universitätsmedizin Berlin and the Berlin Institute of Health. Graphical abstract has been generated using biorender.com.

AUTHOR CONTRIBUTIONS

Conceptualization, A.A.K. and M.-F.M.; methodology, A.A.K., M.-F.M., P.D., L.K., M.D., G.S., M.B., S.A., I.V.S., and V.M.G.; software, P.D.; investigation, M.B., S.A., L.B., P.L., J.N., A.A.K., M.W., J.K., S.M.R., I.S., G.M.G., M.F.-G., E.S.-S., S.Y., T.S., G.A.H., C.T., M.R., D.M., I.V.S., M.D., L.K., and A.L.; resources, J.K., S.M.R., E.S.-S., H.P., E.S., A.-L.S., T.D., S.Z., E.V., N.K., K.J.S., S.T., A.D., and P.E.; writing – original draft, A.A.K., M.W., M.B., L.B., J.N., P.D., M.-F.M., and A.R.; writing – review & editing, M.W., M.B., L.B., J.N., J.K., M.F.-G., S.M.R., M.R., G.S., E.S., A.-L.S., T.D., H.-D.C., M.D., L.K., S.T., A.R., H.P., and P.E.; visualization, A.A.K., P.D., M.B., L.B., and J.N.; project administration, A.A.K., M.-F.M., L.K., P.E., S.T., A.R., A.D., and H.P.; funding acquisition, H.-D.C., A.R., M.-F.M., A.A.K., H.P., V.M.G., J.K., S.M.R., and E.S.

DECLARATION OF INTERESTS

Related to this work, Deutsches Rheuma-Forschungszentrum (DRFZ) has filed a patent application.

INCLUSION AND DIVERSITY

We support inclusive, diverse, and equitable conduct of research.

Received: September 28, 2022
Revised: July 11, 2023
Accepted: October 6, 2023
Published: November 8, 2023

REFERENCES

1. Zhou, P., Yang, X.L., Wang, X.G., Hu, B., Zhang, L., Zhang, W., Si, H.R., Zhu, Y., Li, B., Huang, C.L., et al. (2020). A pneumonia outbreak associated with a new coronavirus of probable bat origin. Nature *579*, 270–273. https://doi.org/10.1038/s41586-020-2012-7.
2. Hoffmann, M., Kleine-Weber, H., Schroeder, S., Krüger, N., Herrler, T., Erichsen, S., Schiergens, T.S., Herrler, G., Wu, N.H., Nitsche, A., et al. (2020). SARS-CoV-2 cell entry depends on ACE2 and TMPRSS2 and is blocked by a clinically proven protease inhibitor. Cell *181*, 271–280.e8. https://doi.org/10.1016/j.cell.2020.02.052.
3. Shang, J., Wan, Y., Luo, C., Ye, G., Geng, Q., Auerbach, A., and Li, F. (2020). Cell entry mechanisms of SARS-CoV-2. Proc. Natl. Acad. Sci. USA *117*, 11727–11734. https://doi.org/10.1073/pnas.2003138117.
4. Walls, A.C., Park, Y.J., Tortorici, M.A., Wall, A., McGuire, A.T., and Veesler, D. (2020). Structure, function, and antigenicity of the SARS-CoV-2 spike glycoprotein. Cell *181*, 281–292.e6. https://doi.org/10.1016/j.cell.2020.02.058.
5. Cao, Y., Su, B., Guo, X., Sun, W., Deng, Y., Bao, L., Zhu, Q., Zhang, X., Zheng, Y., Geng, C., et al. (2020). Potent neutralizing antibodies against SARS-CoV-2 identified by high-throughput single-cell sequencing of convalescent patients' B cells. Cell *182*, 73–84.e16. https://doi.org/10.1016/j.cell.2020.05.025.
6. Ju, B., Zhang, Q., Ge, J., Wang, R., Sun, J., Ge, X., Yu, J., Shan, S., Zhou, B., Song, S., et al. (2020). Human neutralizing antibodies elicited by SARS-CoV-2 infection. Nature *584*, 115–119. https://doi.org/10.1038/s41586-020-2380-z.
7. Renegar, K.B., Small, P.A., Jr., Boykins, L.G., and Wright, P.F. (2004). Role of IgA versus IgG in the control of influenza viral infection in the murine respiratory tract. J. Immunol. *173*, 1978–1986. https://doi.org/10.4049/jimmunol.173.3.1978.
8. Chan, R.W.Y., Liu, S., Cheung, J.Y., Tsun, J.G.S., Chan, K.C., Chan, K.Y.Y., Fung, G.P.G., Li, A.M., and Lam, H.S. (2021). The mucosal and serological immune responses to the novel coronavirus (SARS-CoV-2) vaccines. Front. Immunol. *12*, 744887. https://doi.org/10.3389/fimmu.2021.744887.
9. Macpherson, A.J., Yilmaz, B., Limenitakis, J.P., and Ganal-Vonarburg, S.C. (2018). IgA function in relation to the intestinal microbiota. Annu. Rev. Immunol. *36*, 359–381. https://doi.org/10.1146/annurev-immunol-042617-053238.
10. Tierney, B.T., Yang, Z., Luber, J.M., Beaudin, M., Wibowo, M.C., Baek, C., Mehlenbacher, E., Patel, C.J., and Kostic, A.D. (2019). The landscape of genetic content in the gut and oral human microbiome. Cell Host Microbe *26*, 283–295.e8. https://doi.org/10.1016/j.chom.2019.07.008.
11. Yang, X., Xie, L., Li, Y., and Wei, C. (2009). More than 9,000,000 unique genes in human gut bacterial community: estimating gene numbers inside a human body. PLoS One *4*, e6074. https://doi.org/10.1371/journal.pone.0006074.
12. Zárate-Bladés, C.R., Horai, R., Mattapallil, M.J., Ajami, N.J., Wong, M., Petrosino, J.F., Itoh, K., Chan, C.C., and Caspi, R.R. (2017). Gut microbiota as a source of a surrogate antigen that triggers autoimmunity in an immune privileged site. Gut Microbes *8*, 59–66. https://doi.org/10.1080/19490976.2016.1273996.
13. Gil-Cruz, C., Perez-Shibayama, C., De Martin, A., Ronchi, F., van der Borght, K., Niederer, R., Onder, L., Lütge, M., Novkovic, M., Nindl, V., et al. (2019). Microbiota-derived peptide mimics drive lethal inflammatory cardiomyopathy. Science *366*, 881–886. https://doi.org/10.1126/science.aav3487.
14. Greiling, T.M., Dehner, C., Chen, X., Hughes, K., Iñiguez, A.J., Boccitto, M., Ruiz, D.Z., Renfroe, S.C., Vieira, S.M., Ruff, W.E., et al. (2018). Commensal orthologs of the human autoantigen Ro60 as triggers of autoimmunity in lupus. Sci. Transl. Med. *10*, eaan2306. https://doi.org/10.1126/scitranslmed.aan2306.
15. Ren, Z., Wang, Y., Duan, T., Patel, J., Liggett, T., Loda, E., Brahma, S., Goswami, R., Grouse, C., Byrne, R., et al. (2012). Cross-immunoreactivity between bacterial aquaporin-Z and human aquaporin-4: potential relevance to neuromyelitis optica. J. Immunol. *189*, 4602–4611. https://doi.org/10.4049/jimmunol.1200486.
16. Planas, R., Santos, R., Tomas-Ojer, P., Cruciani, C., Lutterotti, A., Faigle, W., Schaeren-Wiemers, N., Espejo, C., Eixarch, H., Pinilla, C., et al. (2018). GDP-l-fucose synthase is a CD4(+) T cell-specific autoantigen in DRB3*02:02 patients with multiple sclerosis. Sci. Transl. Med. *10*, eaat4301. https://doi.org/10.1126/scitranslmed.aat4301.
17. Bunker, J.J., Erickson, S.A., Flynn, T.M., Henry, C., Koval, J.C., Meisel, M., Jabri, B., Antonopoulos, D.A., Wilson, P.C., and Bendelac, A. (2017). Natural polyreactive IgA antibodies coat the intestinal microbiota. Science *358*, eaan6619. https://doi.org/10.1126/science.aan6619.
18. Robak, O.H., Heimesaat, M.M., Kruglov, A.A., Prepens, S., Ninnemann, J., Gutbier, B., Reppe, K., Hochrein, H., Suter, M., Kirschning, C.J., et al. (2018). Antibiotic treatment-induced secondary IgA deficiency enhances susceptibility to *Pseudomonas aeruginosa* pneumonia. J. Clin. Invest. *128*, 3535–3545. https://doi.org/10.1172/JCI97065.
19. Scott, N.A., Andrusaite, A., Andersen, P., Lawson, M., Alcon-Giner, C., Leclaire, C., Caim, S., Le Gall, G., Shaw, T., Connolly, J.P.R., et al. (2018). Antibiotics induce sustained dysregulation of intestinal T cell immunity by perturbing macrophage homeostasis. Sci. Transl. Med. *10*, eaao4755. https://doi.org/10.1126/scitranslmed.aao4755.
20. Nagao-Kitamoto, H., Leslie, J.L., Kitamoto, S., Jin, C., Thomsson, K.A., Gillilland, M.G., 3rd, Kuffa, P., Goto, Y., Jenq, R.R., Ishii, C., et al. (2020). Interleukin-22-mediated host glycosylation prevents *Clostridioides difficile* infection by modulating the metabolic activity of the gut microbiota. Nat. Med. *26*, 608–617. https://doi.org/10.1038/s41591-020-0764-0.
21. Ichinohe, T., Pang, I.K., Kumamoto, Y., Peaper, D.R., Ho, J.H., Murray, T.S., and Iwasaki, A. (2011). Microbiota regulates immune defense against respiratory tract influenza A virus infection. Proc. Natl. Acad. Sci. USA *108*, 5354–5359. https://doi.org/10.1073/pnas.1019378108.
22. Schaupp, L., Muth, S., Rogell, L., Kofoed-Branzk, M., Melchior, F., Lienenklaus, S., Ganal-Vonarburg, S.C., Klein, M., Guendel, F., Hain, T., et al. (2020). Microbiota-induced Type I interferons instruct a poised basal state of dendritic cells. Cell *181*, 1080–1096.e19. https://doi.org/10.1016/j.cell.2020.04.022.
23. Stefan, K.L., Kim, M.V., Iwasaki, A., and Kasper, D.L. (2020). Commensal microbiota modulation of natural resistance to virus infection. Cell *183*, 1312–1324.e10. https://doi.org/10.1016/j.cell.2020.10.047.
24. Trama, A.M., Moody, M.A., Alam, S.M., Jaeger, F.H., Lockwood, B., Parks, R., Lloyd, K.E., Stolarchuk, C., Scearce, R., Foulger, A., et al. (2014). HIV-1 envelope gp41 antibodies can originate from terminal ileum B cells that share cross-reactivity with commensal bacteria. Cell Host Microbe *16*, 215–226. https://doi.org/10.1016/j.chom.2014.07.003.
25. Williams, W.B., Liao, H.X., Moody, M.A., Kepler, T.B., Alam, S.M., Gao, F., Wiehe, K., Trama, A.M., Jones, K., Zhang, R., et al. (2015). HIV-1 vaccines. Diversion of HIV-1 vaccine-induced immunity by gp41-microbiota cross-reactive antibodies. Science *349*, aab1253. https://doi.org/10.1126/science.aab1253.
26. Ng, K.W., Faulkner, N., Cornish, G.H., Rosa, A., Harvey, R., Hussain, S., Ulferts, R., Earl, C., Wrobel, A.G., Benton, D.J., et al. (2020). Preexisting and de novo humoral immunity to SARS-CoV-2 in humans. Science *370*, 1339–1343. https://doi.org/10.1126/science.abe1107.
27. Simula, E.R., Manca, M.A., Jasemi, S., Uzzau, S., Rubino, S., Manchia, P., Bitti, A., Palermo, M., and Sechi, L.A. (2020). HCoV-NL63 and SARS-CoV-2 share recognized epitopes by the humoral response in sera of people

collected Pre- and during CoV-2 pandemic. Microorganisms *8*, 1993. https://doi.org/10.3390/microorganisms8121993.

28. Majdoubi, A., Michalski, C., O'Connell, S.E., Dada, S., Narpala, S.R., Gelinas, J.P., Mehta, D., Cheung, C., Winkler, D.F., Basappa, M., et al. (2021). A majority of uninfected adults show pre-existing antibody reactivity against SARS-CoV-2. JCI Insight *6*, e146316. https://doi.org/10.1172/jci.insight.146316.
29. Anderson, E.M., Goodwin, E.C., Verma, A., Arevalo, C.P., Bolton, M.J., Weirick, M.E., Gouma, S., McAllister, C.M., Christensen, S.R., Weaver, J., et al. (2021). Seasonal human coronavirus antibodies are boosted upon SARS-CoV-2 infection but not associated with protection. Cell *184*, 1858–1864.e10. https://doi.org/10.1016/j.cell.2021.02.010.
30. Sokal, A., Chappert, P., Barba-Spaeth, G., Roeser, A., Fourati, S., Azzaoui, I., Vandenberghe, A., Fernandez, I., Meola, A., Bouvier-Alias, M., et al. (2021). Maturation and persistence of the anti-SARS-CoV-2 memory B cell response. Cell *184*, 1201–1213.e14. https://doi.org/10.1016/j.cell.2021.01.050.
31. Spiekermann, G.M., Finn, P.W., Ward, E.S., Dumont, J., Dickinson, B.L., Blumberg, R.S., and Lencer, W.I. (2002). Receptor-mediated immunoglobulin G transport across mucosal barriers in adult life: functional expression of FcRn in the mammalian lung. J. Exp. Med. *196*, 303–310. https://doi.org/10.1084/jem.20020400.
32. Wijburg, O.L., Uren, T.K., Simpfendorfer, K., Johansen, F.E., Brandtzaeg, P., and Strugnell, R.A. (2006). Innate secretory antibodies protect against natural Salmonella typhimurium infection. J. Exp. Med. *203*, 21–26. https://doi.org/10.1084/jem.20052093.
33. Sheikh-Mohamed, S., Isho, B., Chao, G.Y.C., Zuo, M., Cohen, C., Lustig, Y., Nahass, G.R., Salomon-Shulman, R.E., Blacker, G., Fazel-Zarandi, M., et al. (2022). Systemic and mucosal IgA responses are variably induced in response to SARS-CoV-2 mRNA vaccination and are associated with protection against subsequent infection. Mucosal Immunol. *15*, 799–808. https://doi.org/10.1038/s41385-022-00511-0.
34. Costello, E.K., Lauber, C.L., Hamady, M., Fierer, N., Gordon, J.I., and Knight, R. (2009). Bacterial community variation in human body habitats across space and time. Science *326*, 1694–1697. https://doi.org/10.1126/science.1177486.
35. Lloyd-Price, J., Mahurkar, A., Rahnavard, G., Crabtree, J., Orvis, J., Hall, A.B., Brady, A., Creasy, H.H., McCracken, C., Giglio, M.G., et al. (2017). Strains, functions and dynamics in the expanded Human Microbiome Project. Nature *550*, 61–66. https://doi.org/10.1038/nature23889.
36. Wang, J., Jia, Z., Zhang, B., Peng, L., and Zhao, F. (2020). Tracing the accumulation of in vivo human oral microbiota elucidates microbial community dynamics at the gateway to the GI tract. Gut *69*, 1355–1356. https://doi.org/10.1136/gutjnl-2019-318977.
37. Eren, A.M., Borisy, G.G., Huse, S.M., and Mark Welch, J.L. (2014). Oligotyping analysis of the human oral microbiome. Proc. Natl. Acad. Sci. USA *111*, E2875–E2884. https://doi.org/10.1073/pnas.1409644111.
38. Bacci, G., Mengoni, A., Emiliani, G., Chiellini, C., Cipriani, E.G., Bianconi, G., Canganella, F., and Fani, R. (2021). Defining the resilience of the human salivary microbiota by a 520-day longitudinal study in a confined environment: the Mars500 mission. Microbiome *9*, 152. https://doi.org/10.1186/s40168-021-01070-5.
39. Yamazaki, A., Ogura, K., Minami, K., Ogai, K., Horiguchi, T., Okamoto, S., and Mukai, K. (2023). Oral microbiome changes associated with the menstrual cycle in healthy young adult females. Front. Cell. Infect. Microbiol. *13*, 1119602. https://doi.org/10.3389/fcimb.2023.1119602.
40. Bondareva, M., Letz, P., Karberg, K., Schrezenmeier, E., Semin, I., Rincon-Arevalo, H., Dörner, T., Mashreghi, M.F., Stefanski, A.L., and Kruglov, A.A. (2022). Induction of cross-reactive, mucosal anti-SARS-CoV-2 antibody responses in rheumatoid arthritis patients after 3rd dose of COVID-19 vaccination. J. Autoimmun. *133*, 102918. https://doi.org/10.1016/j.jaut.2022.102918.
41. Akaishi, T., Takahashi, T., Sato, S., Jin, X., Masamune, A., and Ishii, T. (2022). Prolonged diarrhea following COVID-19 vaccination: A case report and literature review. Tohoku J. Exp. Med. *257*, 251–259. https://doi.org/10.1620/tjem.2022.J043.
42. Kreye, J., Reincke, S.M., Kornau, H.C., Sánchez-Sendin, E., Corman, V.M., Liu, H., Yuan, M., Wu, N.C., Zhu, X., Lee, C.D., et al. (2020). A therapeutic non-self-reactive SARS-CoV-2 antibody protects from lung pathology in a COVID-19 hamster model. Cell *183*, 1058–1069.e19. https://doi.org/10.1016/j.cell.2020.09.049.
43. Wardemann, H., Yurasov, S., Schaefer, A., Young, J.W., Meffre, E., and Nussenzweig, M.C. (2003). Predominant autoantibody production by early human B cell precursors. Science *301*, 1374–1377. https://doi.org/10.1126/science.1086907.
44. Liu, Q., Mak, J.W.Y., Su, Q., Yeoh, Y.K., Lui, G.C., Ng, S.S.S., Zhang, F., Li, A.Y.L., Lu, W., Hui, D.S., et al. (2022). Gut microbiota dynamics in a prospective cohort of patients with post-acute COVID-19 syndrome. Gut *71*, 544–552. https://doi.org/10.1136/gutjnl-2021-325989.
45. Barretto, C., Alvarez-Martin, P., Foata, F., Renault, P., and Berger, B. (2012). Genome sequence of the lantibiotic bacteriocin producer Streptococcus salivarius strain K12. J. Bacteriol. *194*, 5959–5960. https://doi.org/10.1128/JB.01268-12.
46. Kozlovskaya, L.I., Piniaeva, A.N., Ignatyev, G.M., Gordeychuk, I.V., Volok, V.P., Rogova, Y.V., Shishova, A.A., Kovpak, A.A., Ivin, Y.Y., Antonova, L.P., et al. (2021). Long-term humoral immunogenicity, safety and protective efficacy of inactivated vaccine against COVID-19 (CoviVac) in preclinical studies. Emerg. Microbes Infect. *10*, 1790–1806. https://doi.org/10.1080/22221751.2021.1971569.
47. Lynn, D.J., Benson, S.C., Lynn, M.A., and Pulendran, B. (2022). Modulation of immune responses to vaccination by the microbiota: implications and potential mechanisms. Nat. Rev. Immunol. *22*, 33–46. https://doi.org/10.1038/s41577-021-00554-7.
48. Geva-Zatorsky, N., Sefik, E., Kua, L., Pasman, L., Tan, T.G., Ortiz-Lopez, A., Yanortsang, T.B., Yang, L., Jupp, R., Mathis, D., et al. (2017). Mining the human gut microbiota for immunomodulatory organisms. Cell *168*, 928–943.e11. https://doi.org/10.1016/j.cell.2017.01.022.
49. Bradley, K.C., Finsterbusch, K., Schnepf, D., Crotta, S., Llorian, M., Davidson, S., Fuchs, S.Y., Staeheli, P., and Wack, A. (2019). Microbiota-driven tonic interferon signals in lung stromal cells protect from influenza virus infection. Cell Rep. *28*, 245–256.e4. https://doi.org/10.1016/j.celrep.2019.05.105.
50. Ferreira-Gomes, M., Kruglov, A., Durek, P., Heinrich, F., Tizian, C., Heinz, G.A., Pascual-Reguant, A., Du, W., Mothes, R., Fan, C., et al. (2021). SARS-CoV-2 in severe COVID-19 induces a TGF-beta-dominated chronic immune response that does not target itself. Nat. Commun. *12*, 1961. https://doi.org/10.1038/s41467-021-22210-3.
51. Beller, A., Kruglov, A., Durek, P., von Goetze, V., Werner, K., Heinz, G.A., Ninnemann, J., Lehmann, K., Maier, R., Hoffmann, U., et al. (2020). Specific microbiota enhances intestinal IgA levels by inducing TGF-beta in T follicular helper cells of Peyer's patches in mice. Eur. J. Immunol. *50*, 783–794. https://doi.org/10.1002/eji.201948474.
52. Donaldson, G.P., Ladinsky, M.S., Yu, K.B., Sanders, J.G., Yoo, B.B., Chou, W.C., Conner, M.E., Earl, A.M., Knight, R., Bjorkman, P.J., and Mazmanian, S.K. (2018). Gut microbiota utilize immunoglobulin A for mucosal colonization. Science *360*, 795–800. https://doi.org/10.1126/science.aaq0926.
53. Jeffries, T.L., Jr., Sacha, C.R., Pollara, J., Himes, J., Jaeger, F.H., Dennison, S.M., McGuire, E., Kunz, E., Eudailey, J.A., Trama, A.M., et al. (2016). The function and affinity maturation of HIV-1 gp120-specific monoclonal antibodies derived from colostral B cells. Mucosal Immunol. *9*, 414–427. https://doi.org/10.1038/mi.2015.70.
54. Dl Pierro, F., and Colombo, M. (2021). The administration of S. salivarius K12 to children may reduce the rate of SARS-CoV-2 infection. Minerva Med. *112*, 514–516. https://doi.org/10.23736/S0026-4806.21.07487-5.
55. Di Pierro, F., Iqtadar, S., Mumtaz, S.U., Bertuccioli, A., Recchia, M., Zerbinati, N., and Khan, A. (2022). Clinical effects of *Streptococcus salivarius* K12 in Hospitalized COVID-19 patients: results of a preliminary

study. Microorganisms *10*, 1926. https://doi.org/10.3390/microorganisms10101926.

56. Fajnzylber, J., Regan, J., Coxen, K., Corry, H., Wong, C., Rosenthal, A., Worrall, D., Giguel, F., Piechocka-Trocha, A., Atyeo, C., et al. (2020). SARS-CoV-2 viral load is associated with increased disease severity and mortality. Nat. Commun. *11*, 5493. https://doi.org/10.1038/s41467-020-19057-5.

57. Liu, Y., Yan, L.M., Wan, L., Xiang, T.X., Le, A., Liu, J.M., Peiris, M., Poon, L.L.M., and Zhang, W. (2020). Viral dynamics in mild and severe cases of COVID-19. Lancet Infect. Dis. *20*, 656–657. https://doi.org/10.1016/S1473-3099(20)30232-2.

58. Yeoh, Y.K., Zuo, T., Lui, G.C., Zhang, F., Liu, Q., Li, A.Y., Chung, A.C., Cheung, C.P., Tso, E.Y., Fung, K.S., et al. (2021). Gut microbiota composition reflects disease severity and dysfunctional immune responses in patients with COVID-19. Gut *70*, 698–706. https://doi.org/10.1136/gutjnl-2020-323020.

59. Zuo, T., Zhang, F., Lui, G.C.Y., Yeoh, Y.K., Li, A.Y.L., Zhan, H., Wan, Y., Chung, A.C.K., Cheung, C.P., Chen, N., et al. (2020). Alterations in gut microbiota of patients with COVID-19 during time of hospitalization. Gastroenterology *159*, 944–955.e8. https://doi.org/10.1053/j.gastro.2020.05.048.

60. Gu, S., Chen, Y., Wu, Z., Chen, Y., Gao, H., Lv, L., Guo, F., Zhang, X., Luo, R., Huang, C., et al. (2020). Alterations of the gut microbiota in patients with COVID-19 or H1N1 influenza. Clin. Infect. Dis. *71*, 2669–2678. https://doi.org/10.1093/cid/ciaa709.

61. Ma, S., Zhang, F., Zhou, F., Li, H., Ge, W., Gan, R., Nie, H., Li, B., Wang, Y., Wu, M., et al. (2021). Metagenomic analysis reveals oropharyngeal microbiota alterations in patients with COVID-19. Signal Transduct. Target. Ther. *6*, 191. https://doi.org/10.1038/s41392-021-00614-3.

62. Sulaiman, I., Chung, M., Angel, L., Tsay, J.J., Wu, B.G., Yeung, S.T., Krolikowski, K., Li, Y., Duerr, R., Schluger, R., et al. (2021). Microbial signatures in the lower airways of mechanically ventilated COVID-19 patients associated with poor clinical outcome. Nat. Microbiol. *6*, 1245–1258. https://doi.org/10.1038/s41564-021-00961-5.

63. Devi, P., Kumari, P., Yadav, A., Tarai, B., Budhiraja, S., Shamim, U., and Pandey, R. (2023). Transcriptionally active nasopharyngeal commensals and opportunistic microbial dynamics define mild symptoms in the COVID 19 vaccination breakthroughs. PLoS Pathog. *19*, e1011160. https://doi.org/10.1371/journal.ppat.1011160.

64. Cui, G.Y., Rao, B.C., Zeng, Z.H., Wang, X.M., Ren, T., Wang, H.Y., Luo, H., Ren, H.Y., Liu, C., Ding, S.Y., et al. (2022). Characterization of oral and gut microbiome and plasma metabolomics in COVID-19 patients after 1-year follow-up. Mil. Med Res *9*, 32. https://doi.org/10.1186/s40779-022-00387-y.

65. Ng, S.C., Peng, Y., Zhang, L., Mok, C.K., Zhao, S., Li, A., Ching, J.Y., Liu, Y., Yan, S., Chan, D.L.S., et al. (2022). Gut microbiota composition is associated with SARS-CoV-2 vaccine immunogenicity and adverse events. Gut *71*, 1106–1116. https://doi.org/10.1136/gutjnl-2021-326563.

66. Uehara, O., Abiko, Y., Nagasawa, T., Morikawa, T., Hiraki, D., Harada, F., Kawano, Y., Toraya, S., Matsuoka, H., Paudel, D., et al. (2022). Alterations in the oral microbiome of individuals with a healthy oral environment following COVID-19 vaccination. BMC Oral Health *22*, 50. https://doi.org/10.1186/s12903-022-02093-6.

67. Woo, P.C., Leung, P.K., Leung, K.W., and Yuen, K.Y. (2000). Identification by 16S ribosomal RNA gene sequencing of an Enterobacteriaceae species from a bone marrow transplant recipient. Mol. Pathol. *53*, 211–215. https://doi.org/10.1136/mp.53.4.211.

68. Masella, A.P., Bartram, A.K., Truszkowski, J.M., Brown, D.G., and Neufeld, J.D. (2012). PANDAseq: paired-end assembler for Illumina sequences. BMC Bioinformatics *13*, 31. https://doi.org/10.1186/1471-2105-13-31.

69. Cole, J.R., Wang, Q., Fish, J.A., Chai, B., McGarrell, D.M., Sun, Y., Brown, C.T., Porras-Alfaro, A., Kuske, C.R., and Tiedje, J.M. (2014). Ribosomal Database Project: data and tools for high throughput rRNA analysis. Nucleic Acids Res. *42*, D633–D642. https://doi.org/10.1093/nar/gkt1244.

70. Wang, Q., Garrity, G.M., Tiedje, J.M., and Cole, J.R. (2007). Naive Bayesian classifier for rapid assignment of rRNA sequences into the new bacterial taxonomy. Appl. Environ. Microbiol. *73*, 5261–5267. https://doi.org/10.1128/AEM.00062-07.

71. McMurdie, P.J., and Holmes, S. (2013). phyloseq: an R package for reproducible interactive analysis and graphics of microbiome census data. PLoS One *8*, e61217. https://doi.org/10.1371/journal.pone.0061217.

72. Jari Oksanen, F.G.B., Friendly, M., Kindt, R., Legendre, P., McGlinn, D., Minchin, P.R., O'Hara, R.B., Simpson, G.L., Solymos, P., Henry, M., et al. (2020). vegan: community Ecology Package. https://CRAN.R-project.org/packahe=vegan.

73. Segata, N., Izard, J., Waldron, L., Gevers, D., Miropolsky, L., Garrett, W.S., and Huttenhower, C. (2011). Metagenomic biomarker discovery and explanation. Genome Biol. *12*, R60. https://doi.org/10.1186/gb-2011-12-6-r60.

74. Sayers, E.W., Beck, J., Bolton, E.E., Bourexis, D., Brister, J.R., Canese, K., Comeau, D.C., Funk, K., Kim, S., Klimke, W., et al. (2021). Database resources of the National Center for Biotechnology Information. Nucleic Acids Res. *49*, D10–D17. https://doi.org/10.1093/nar/gkaa892.

75. Eren, A.M., Morrison, H.G., Lescault, P.J., Reveillaud, J., Vineis, J.H., and Sogin, M.L. (2015). Minimum entropy decomposition: unsupervised oligotyping for sensitive partitioning of high-throughput marker gene sequences. ISME J. *9*, 968–979. https://doi.org/10.1038/ismej.2014.195.

76. Klindworth, A., Pruesse, E., Schweer, T., Peplies, J., Quast, C., Horn, M., and Glöckner, F.O. (2013). Evaluation of general 16S ribosomal RNA gene PCR primers for classical and next-generation sequencing-based diversity studies. Nucleic Acids Res. *41*, e1. https://doi.org/10.1093/nar/gks808.

STAR★METHODS

KEY RESOURCES TABLE

REAGENT or RESOURCE	SOURCE	IDENTIFIER
Antibodies		
Anti-human IgA1 Alexa Fluor 647 (clone: B3506B4)	Southern Biotech	Cat. No. 9130-31; RRID: AB_2796658
Anti-human IgA2 Alexa Fluor 488 (clone: A9604D2)	Southern Biotech	Cat. No. 9140-30; RRID: AB_2796665
Rabbit SARS-CoV-2 Spike Neutralizing Antibody (clone: HA14JL2302)	Sino Biological Inc.	Cat. No: 40592-R001; RRID: AB_2857936
Neutralizing Antibody isolated from COVID-19 patients	Kreye et al.[42]	PMID: 33058755
Anti-rabbit IgG Alexa647	Jackson ImmunoResearch	Cat. No. 111-606-144; RRID: AB_2338083
PE/Dazzle™ 594 anti-human IgG Fc Recombinant	BioLegend	Cat. No.: 366920; RRID: AB_2890798
Goat anti-human Ig (H+L chain) antibody	Southern Biotech	Cat. No. 2010-01; RRID: AB_2687525
Goat anti-human IgA Fab	Southern Biotech	Cat. No. 2050-01; RRID: AB_2795701
Biotinylated anti-human IgA antibody	Southern Biotech	Cat. No. 2050-08; RRID: AB_2795706
Anti-human IgG-AP	ICN/Cappel	Cat No. 59289; RRID: AB_2334819
Anti-human IgA-AP	Sigma-Aldrich	Cat.No. A2043; RRID: AB_1839770
Anti-SARS-CoV-2 Spike Glycoprotein S1 antibody (clone: CR3022)	Abcam	Cat. No. ab273073; RRID: AB_2848080
Anti-human IgA FITC	Sothern Biotech	Cat. No. 2052-02; RRID: AB_2795710
Anti-rabbit Alexa 647	Jackson ImmunoResearch	Cat. No. 111-606-144; RRID: AB_2338083
Anti-Mouse IgA Antibody DyLight® 650	Bethyl Laboratories	Cat.No.: A90-103D5; RRID: AB_10630982
Rabbit neutralizing anti-RBD antibody	Sino Biological Inc.	Cat. No. 40592-R001; RRID: AB_2857936
Anti-rabbit IgG-HRP	Cell signaling	Cat. No. 7074S; RRID: AB_2099233
Anti-human IgG-HRP	Southern Biotech	Cat. No. 2040-05; RRID: AB_2795644
Bacterial and virus strains		
Rosetta DE3	Sigma-Aldrich	Cat. No. 70954-3
Chemically competent *E.coli* TOP10	In house	N/A
Streptococcus salivarius K12	Novozin immun	Cat. No. 18170211
Streptococcus salivarius	This paper	N/A
Sterptococcus australis/ Rubner	This paper	N/A
Streptococcus parasanguinis	This paper	N/A
Escherichia Coli	This paper	N/A
Bacillus safensis	This paper	N/A
Bacillus cereus	This paper	N/A
Escherichia fergusonii	This paper	N/A
Bifidobacterium pseudocatenulatum	This paper	N/A
Bifidobacterium longum	This paper	N/A
Enterococcus hirae	This paper	N/A
Enterococcus faecalis	This paper	N/A
Acidaminococcus intestinalis	This paper	N/A
Veillonella parvula	This paper	N/A
Whole-virion inactivated SARS-CoV-2 vaccine	Kozlovskaya et al.[46]	PMID: 34427172
Biological samples		
Human fecal samples	This paper	N/A
Human saliva samples	This paper	N/A
Human serum samples	This paper	N/A
Human swab samples	This paper	N/A
Murine fecal samples	This paper	N/A
Murine serum samples	This paper	N/A

(*Continued on next page*)

Continued

REAGENT or RESOURCE	SOURCE	IDENTIFIER
Murine lung samples	This paper	N/A
Chemicals, peptides, and recombinant proteins		
DNase I	Sigma Aldrich	Cat. No. 10104159001
KAPA HiFi HotStart ReadyMix	Roche	Cat. No. 07958935001
Taq-polymerase	Rapidozym GmbH	Cat. No. GEN-003-1000
dNTP mix	Thermo Fisher Scientific	Cat. No. R0192
AmPure XP Beads	Beckman Coulter Life Science	Cat. No. A63881
Hoechst 33342 solution	Thermo Fisher Scientific	Cat. No. 62249
Sphero™ Rainbow Particles	BD Biosciences	Cat. No. 559123
Accudrop Beads BD	Biosciences	Cat. No. 345249
DEPC treated water	Invitrogen	Cat. No. 46-2224
Brain heart infusion broth	Sigma	Cat. No. 53286-100G
Fastidious agar plates	Thermo Fisher Scientific	Cat. No. 12957138
Schaedler broth	Roth	Cat. No. 5772.1
LB medium	MP Biomedicals	Cat. No. 113002032
2xTY medium	MP Biomedicals	Cat. No. 113012031
PYG MEDIUM (modified)	DSMZ	www.dsmz.de
Isopropyl β- d-1-thiogalactopyranoside (IPTG)	Invitrogen	Cat. No. 15529019
Restrictase *NdeI*	New England BioLabs	Cat. No. R0111S
Restrictase *XhoI*	New England BioLabs	Cat. No. R0146S
Recombinant Uncharacterised protein RSSL-01370	This paper	N/A
HisPur™ Cobalt resin	Thermo Fisher Scientific	Cat. No. 89964
Human IgA	Genway	Cat. No. E04696
Human IgG	Jackson ImmunoResearch	Cat. No- 111-606-144
pNPP	Sigma-Aldrich	Cat. No. N2770
Streptavidin-HRP	Invitrogen	Cat. No. 88-7324-88
Tetramethylbenzidine (TMB) Substrate	Invitrogen	Cat. No. 88-7324-88
Sulfuric acid 25%	Sigma-Aldrich	Cat. No. 1007161000
Sodium hydroxide	Roth	Cat. No. 6771.1
SARS-CoV-2 Spike S1 Subunit His-tag Protein	R&D	Cat. No. 10522-CV
SARS-CoV-2 (2019-nCoV) Spike Protein (RBD, His Tag)	Sino biological	Cat. No. 40592-V08B-100
SARS-CoV-2 Nucleocapsid His Protein, CF	R&D	Cat. No. 10474-CV
SARS-CoV-2 Spike RBD protein (flag-his) (Omicron/B.1.1.529)	SanyouBio	Cat. No. PNA055
RBD peptide ($RBD_{480-496}$: CNGVEGFNCYFPLQSYG)	Eurogentek	Cat. No: AS-65619
Recombinant SARS-CoV-2 S Protein RBD-Fc Chimera (carrier-free)	BioLegend	Cat. No. 793106
Fixable Viability Dye eFluor 450	Invitrogen	Cat. No. 50-112-8817
ACE2 protein	Southern Biotech	Cat. No. 2010-01
Biotinylated RBD	Miltenyi Biotec	Cat No: 130-127-457
Protease inhibitors cocktail	Roche	Cat. No. 11 836 145 001
glass beads	MP Biomedicals	Cat. No. 6911100
non-fat milk	Roth	Cat. No. 68514-61-4
SuperSignal West Fempto Maximum Sensitivity	Thermo Fisher scientific	Cat No. 34095
Trypsin (Trypsin Gold, Mass Spectrometry Grade)	Promega	Cat. No. V5280
2,5-dihydroxybenzoic acid	Sigma-Aldrich	Cat. No. 149357
Ampicillin	Thermo Fisher scientific	Cat. No. 11593027
Polyethylene glycol	Sigma-Aldrich	Cat. No. P7181
HAT Media Supplement (50×) Hybri-Max	Sigma-Aldrich	Cat. No. H0262-10VL

(*Continued on next page*)

Continued

REAGENT or RESOURCE	SOURCE	IDENTIFIER
Alum	Thermo Fisher Scientific	Cat. No. 77161
Lipofectamine 2000	Thermo Fisher Scientific	Cat. No. 11668019
Critical commercial assays		
NGS standard sensitivity fragment analysis kit	Agilent	Cat. No. DF-473-1000
Nextera XT Index Kit v2 Set C/D	Illumina	Cat. No. FC-131-2003
MiSeq Reagent Kit v3 (600 cycle)	Illumina	Cat. No. MS1023003
NucleoSpin Gel and PCR Clean-up Kit	Macherey-Nagel	Cat. No. 740609.50
Quick-DNA™ Fecal/Soil Microbe Miniprep Kit	Zymo Research	Cat. No. D6010
Peptide microarray multiwell replitope SARS-CoV-2 Spike glycoprotein wild type + mutations	JPT Peptide Technologies GmbH	Cat. No. RT-MW-WCPV-S-V02
Easy Stool Extraction Device	ALPCO	Cat. No. 30-EZEX-100
Deposited data		
Raw sequence data	NCBI Sequence Read Archive (SRA)	Bioproject: PRJNA738291
Experimental models: Cell lines		
HEK293T cells	Ferreira-Gomes et al.[50]	PMID: 33785765; RRID:CVCL_0063
Vero cells	Kozlovskaya et al.[46]	PMID: 34427172; RRID:CVCL_0574
P3X63Ag8.653 myeloma cells	ATCC	Cat. No. CRL-1580; RRID:CVCL_4032
Experimental models: Organisms/strains		
Hemizygous K18-hACE2 Tg mice (B6.Cg-Tg (K18-ACE2)2Prlmn/J) on C57Bl/6 genetic background	Jackson Laboratory	JAX #034860, RRID:IMSR_JAX:034860
C57BL/6J	Jackson Laboratory	JAX #000664, RRID:IMSR_JAX:000664
Oligonucleotides		
16S Amplicon PCR Forward Primer 5'-TCgTCggCAg CgTCAgATgTgTATAAgAgACAgCCTAC gggNggCWgCAg-3'	Klindworth et al.[76]	PMID: 22933715
16S Amplicon PCR Reverse Primer 5'-gTCTCgTggg CTCggAgATgTgTATAAgAgACAggACTACHVggg TATCTAATCC-3'	Klindworth et al.[76]	PMID: 22933715
LPW57 5'-AgTTTgATCCTggCTCAg-3'	Woo et al.[67]	PMID: 11040945
LPW58 5'-AGgCCCgggAACgTATTCAC-3'	Woo et al.[67]	PMID: 11040945
Uncharacterised protein RSSL-01370 Forward Primer 5'- CTCCATATgAATTTACCAAgTCACCATACAAggg -'3	This paper	N/A
Uncharacterised protein RSSL-01370 Reverse Primer 5'- gTggTCgACATTCACTTTTTCAgTTgCTACACC -'3	This paper	N/A
Recombinant DNA		
pET-21b expression vector	Addgene	Cat. No. 69741-3
pCG1-SARS-CoV-2-S	Hoffmann et al.[2]	PMID: 32142651
Software and algorithms		
MiSeq Reporter Software	Illumina	www.illumina.com
PANDAseq 2.11	GitHub	www.github.com
Graphpad Prism 9.3.1	Prism	https://www.graphpad.com
FlowJo v10	Tree Star Inc.	www.flowjo.com
Mascot MS/MS ion search	Matrix Science	www.matrixscience.com
Biotools software	Bruker Daltonik	www.bruker.com
ZEN 2.0	Carl Zeiss AG	N/A
Other		
Easy Stool Extraction Device	ALPCO	Cat. No. 30-EZEX-100
Agilent Fragment Analyzer 5200	Roche	Cat. No. M5310AA

(*Continued on next page*)

Continued

REAGENT or RESOURCE	SOURCE	IDENTIFIER
Illumina MySeq 2500	Illumina	www.illumina.com
Spectramax plus 384	Molecular devices	Cat. No. 5510-236-04
COY anaerobic chamber	COY Lab products	www.coylab.com
BD Influx®	BD Biosciences	www.bdbiosciences.com
FACSCanto II	BD Biosciences	www.bdbiosciences.com
MACS Quant 16	Miltenyi Biotec	www.miltenyibiotec.com
Microarray scanner Innoscan 710.	Innopsys	www.innopsys.com
Chemi Doc XRS+ imaging system	Bio-Rad	Cat. No. 1708265
Ultraflex II MALDI-ToF-ToF mass spectrometer	Bruker Daltonik	www.bruker.com
Cryotome MH560	Thermo Fisher Scientific	www.assets.thermofisher.com
LSM 880	Carl Zeiss AG	N/A

RESOURCE AVAILABILITY

Lead contact

Further information and requests for resources and reagents should be directed to and will be fulfilled by the lead contact, Andrey Kruglov (kruglov@drfz.de).

Materials availability

Plasmids, cell lines and antibodies, bacterial strains generated during the study are available upon request to the lead contact.

Data and code availability

- Microbiota 16S sequencing data have been deposited at NCBI Sequence Read Archive (SRA) and will be publicly available by the date of publication. Accession numbers are listed in the key resources table. Original western blot images are included in the manuscript. The DOI is listed in the key resources table. Microscopy data reported in this paper will be shared by the lead contact upon request.
- No original code has been generated during this study.
- Any additional information required to reanalyze the data reported in this paper is available from the lead contact upon request.

EXPERIMENTAL MODEL AND STUDY PARTICIPANT DETAILS

Human Donors

Healthy individuals within BNT162b2 vaccination study were consented within the BNT162-01 study (ClinicalTrials.gov Identifier: NCT04380701) and informed consent forms are archived as per 162-01 procedures. Table S1 reports median age and sex proportions among the participants. Other individuals participating in this study gave written informed consent according to the approval of the ethics committee at the Charité University Hospital Berlin (EA4/019/21, EA2/200/21, EA2/010/21, EA2/066/20, EA4/188/20 and EA2/002/21) and was in compliance with the Declaration of Helsinki. Tables S3, S4, S6, and S7 reports median age, sex proportions and treatments regimes among the participants. Table S2 reports characteristics of rheumatoid arthritis patients enrolled in the analysis of oral microbiota after vaccination with the median of age, sex proportions, and medications. Table S8 reports median age, sex proportions and treatments regimes among the participants suffering from respiratory infections, COVID-19 infection was confirmed by respective PCR analysis for SARS-CoV-2 RNA. All the participants gave informed consent to participate in the study before taking part.

Supplementation of healthy individuals with probiotic bacteria

Healthy volunteers were recruited. Inclusion criteria were: full course of vaccination against SARS-CoV-2, with the time after last vaccination being more than 3 months (Figure 6) or unvaccinated (Figure S15; Table S7). Participants were provided with 50 mg (10^7 CFU) of *Streptococcus salivarius K12* (Novozin immun; Bluestone pharma) which was taken once per day before sleep. Control participants were not provided with any additional supplements. Serum and saliva were collected and analyzed for anti-Spike antibody titers at day 0 and day 14 of probiotic supplementation. Anti-nucleocapsid IgG titers were measured at day 0 and day 14 of the study to exclude the exposure of participants to SARS-CoV-2 during the study.

Mice

Hemizygous K18-hACE2 Tg mice (B6.Cg-Tg(K18-ACE2)2Prlmn/J) on C57Bl/6 genetic background were purchased from the Jackson Laboratory (JAX #034860, RRID:IMSR_JAX:034860). Wild type C57Bl/6 mice were acquired from the Pushchino Animal Breeding

Facility (Branch of the Shemyakin and Ovchinnikov Institute of Bioorganic Chemistry, Russian Academy of Sciences). All animals were maintained under SPF conditions at the Center for Collective Use of the Institute of Physiologically Active Compounds or the Center for Precision Genome Editing and Genetic Technologies for Biomedicine, Engelhardt Institute of Molecular Biology, Russian Academy of Sciences. All animal procedures were performed in accordance with Russian regulations of animal protection and approved by the local Ethics Review Committees at the Institute of Physiologically Active Compounds RAS (protocol No 50, August 10, 2020) and the Engelhardt Institute of Molecular Biology RAS (protocol No 2, September 14, 2022).

Mice immunizations

Grown bacteria were collected, washed three times with PBS and heat-inactivated at 65 °C for 1 hr. Heat inactivated bacteria were resuspended with final OD_{600} equals 1.0. C57Bl/6 mice (8-12 weeks, both males and females) were injected with 200 μl of heat-killed bacteria i.p. From oral gavage, live bacteria stocks were grown, washed with PBS several times, OD_{600} was adjusted to 1, 200 μl of live bacteria was gavaged every day. For the immunization with the uncharacterized protein RSSL-01370 recombinant protein RSSL-01370 was produced in *E.coli* and purified (see corresponding section in STAR Methods). 20 μg per mouse (C57Bl/6 strain, 8-12 weeks old, females) was injected intraperitoneally as a mixture with Alum 1:1, v/v (Thermo Scientific, Cat. No. 77161). Boost immunization was done at day 14 after primary injection. All animal procedures were performed in accordance with Russian regulations of animal protection.

Mice vaccination and infection

Whole-virion inactivated SARS-CoV-2 vaccine (CoviVac) was produced from the prototype B.1.1 SARS-CoV-2 strain (GISAID ID EPI_ISL_428851) in Vero cells.[46] K18-hACE2 Tg (8-12 weeks, both males and females) were vaccinated intramuscularly with CoviVac vaccine or intraperitoneally with alum or bacteria mixture emulsified in alum at day 0 and day 14.[46] At day 21, K18-hACE2 Tg mice were infected intranasally at 10^4 $TCID_{50}$ (25 μL into each nostril) with B.1.1 SARS-CoV-2 one week following the second vaccination with CoviVac or Alum (Thermo Scientific, Cat. No. 77161). Animals were clinically examined and weighed daily. On day 7 of infection mice were sacrificed.

Bacteria culture

PYG medium and plates were prepared as described by the DSMZ (German Collection of Microorganisms and Cell Cultures). 300,000 events were sorted into 1 ml of PYG medium and directly transferred to a COY anaerobic chamber. Sorted bacteria were plated on PYG, BHI (Brain heart infusion broth, Sigma, Cat. No. 53286-100G) and Fastidious agar plates (Thermo Fisher Scientific, Cat. No. 12957138) and bacteria were grown for 24 hours. Colonies were picked and PYG medium, BHI broth and Schaedler broth (Roth, Cat. No. 5772.1) were inoculated with colonies from the respective plates. The next day, DNA was isolated and the remaining bacteria were frozen in 40% glycerol LB medium in liquid nitrogen or – 80 °C.

METHOD DETAILS

Swabs and saliva sample preparation

Whole saliva was collected in collection tubes and centrifuged at 2000g for 15 min at +4°C. Supernatant was stored at -80 °C for further analysis. Saliva pellets were further used for 16S rDNA sequencing similarly to the swab samples. Swabs were prepared for 16S rDNA sequencing with an adapted protocol of the Quick-DNA™ Fecal/Soil Microbe Miniprep Kit (Zymo Research, Cat. No. D6010). Swabs were obtained from clinics at – 80 °C and kept frozen until further use. The swab stick was either already stored in buffer or Bead Bashing™ buffer was added to cover the swab brush. Up to 750 μL of the buffer solutions were transferred to a BashingBead™ Lysis Tube and rigorously mixed at 13,000 rpm at 37 °C. Following the kits protocol, the supernatant was harvested after centrifugation at 13,000 x g for 5 min and once more filtered by Zymo-Spin™ III-F Filter. The DNA containing solution was then treated with Genomic Lysis Buffer and the containing DNA was put on a DNA binding Zymo-Spin™ IICR Column repeatedly until the entire sample volume was loaded. The bound DNA was washed with DNA Pre-Wash Buffer and g-DNA Wash Buffer. The washed DNA was eluted in 50 μL DNA Elution buffer and once further purified by filtration through the Zymo-Spin™ III-HRC Filter. 2.5 μL of each of the prepared samples was directly loaded to the amplicon PCR of the Illumina Nextera NGS protocol described in the 16S rRNA method section.

Stool sample preparation from BNT162b2 vaccinated individuals

Fresh stool samples from participants were collected using ALPCO Easy Stool Extraction Device according to the manufacturer's instructions and were stored at -80°C before processing. Thawed stool suspensions were filtered through 70 μm (Falcon, Cat. No. 352350) and 30 μm filters (CellTrics®, Sysmex, Cat. No. 04-0042-2316) and centrifuged at 4000 x g to pellet the bacterial cells. Bacteria-free supernatant was filtered through a 0.22 μm syringe top (Filtropur, Sarstedt Cat. No. 83.1826.001) filter and stored at – 80°C until further use. Pellets were resuspended in 1 mL of a 40 % glycerol in LB medium mixture in Safe Seal 2 mL reaction tubes (Sarstedt, Cat. No. 72.695.500) and stored at – 80°C.

Stool sample preparation for bacteria isolation

Fresh stool samples from healthy controls were stored on ice or at 4°C before processing within 48 h. The stool was diluted in autoclaved and sterile-filtered PBS (in-house, Steritop® Millipore Express®PLUS 0.22 μm, Cat. No: 2GPT05RE) according to weight in

the ratio 100 μg/mL and homogenized by vortex and spatula. The feces solution was then subsequently filtered through 70 μm (Falcon, Cat. No. 352350) and 30 μm filters (CellTrics®, Sysmex, Cat. No. 04-0042-2316) and centrifuged at 4000 x g to pellet the bacterial cells. The supernatant of this centrifugation step was once more centrifuged at 13,000 x g to pellet residual cells. The cell free supernatant was filtered through a 0.22 μm syringe top (Filtropur, Sarstedt Cat. No. 83.1826.001) filter and stored at – 80°C until further use. Pellets of both centrifugation steps were pooled and re-suspended in 10 mL PBS to measure the cell density at 600 nm. For each working stock a cell amount resembling 0.4 OD was stored in 1 mL of a 40 % glycerol in LB medium mixture in Safe Seal 2 mL reaction tubes (Sarstedt, Cat. No. 72.695.500) and transferred to – 80°C.

16S rRNA gene sequencing and analysis

For 16 S rRNA gene sequencing, we amplified the V3/V4 region directly from the bulk microbiota samples and from the sorted samples (primer sequences: 5'-TCgTCggCAgCgTCAgATgTgTATAAgAgACAgCCTACgggNggCWgCAg-3' and 5'-gTCTCgTgggCTCggAgATgTgTATAAgAgACAggACTACHVgggTATCTAATCC-3') with a prolonged initial heating step as described by ''16S Metagenomic Sequencing Library Preparation'' for the Illumina MiSeq System. After the amplicon the genomic DNA was removed by AmPure XP Beads (Beckman Coulter Life Science Cat. No. A63881) with a 1:1.25 ratio of sample to beads (v/v). Next the amplicons were checked for their size and purity on a 1.5 % agarose gel and if suitable subjected to the index PCR using the Nextera XT Index Kit v2 Set C/D (Illumina, FC-131-2003). After index PCR the samples were cleaned again with AmPure XP Beads (Beckman Coulter Life Science Cat. No. A63881) in a 1: 0.8 ratio of sample to beads (v/v). Samples were then analyzed by capillary gel electrophoresis (Agilent Fragment Analyzer 5200) for correct size and purity with the NGS standard sensitivity fragment analysis kit (Agilent Cat. No. DF-473). Of all suitable samples a pool of 2 nM was generated and loaded to the Illumina MySeq 2500 system.

Raw data were processed and de-multiplexed using MiSeq Reporter Software. Forward and reverse reads were combined using PANDAseq 2.11 with a minimum overlap of 25 bases[68] and classified using ''classifier.jar'' 2.13 from the Ribosomal Database Project with a confidence cutoff of 50%.[69,70] The copy number adjusted counts were agglomerated to bacterial genera, rarefied to the smallest size and alpha diversity were estimated using phyloSeq 1.34.[71] Principle coordinate analysis were performed using Bray–Curtis dissimilarity distance using vegan 2.5-7.[72]

The linear discriminant analysis were performed using LEfSe, based on copy number adjusted counts normalized to 1M reads.[73] Raw sequence data were deposited at the NCBI Sequence Read Archive (SRA) under the accession number PRJNA738291.

Two approaches were performed to refine the classification of the Streptococcus on genus level: annotation of the underlying species based on similarities to NCBI's 16S ribosomal RNA sequences[74] as well as unsupervised oligotyping based on minimum entropy decomposition (MED).[37,75] Both approaches were performed for reads assigned to the Streptococcus by the RDP classifier. For the similarity based approach a basic local alignment search was performed using megablast to retrieve 100 best hits. Because of the high similarity of the sequences from different Streptococcus species reaching up to 100% identity, the taxa of the best hits in case of equal identities were assigned in contrast to the lowest common ancestor classification. The oligotyping approach was based on pairwise sequence alignments between the Streptococcus reads and the 300-764 Region of a Streptococcus vulneris reference (NCBI Reference Sequence:NR_179383.1) using the Needleman Wunsch algorithm. The aligned sequences were aligned by keeping gaps and removing potential insertions to generate the multiple alignment. The minimal entropy decomposition was performed as described by Eren et al. using a critical entropy above 0.6 to split oligotypes and not considering gaps or potential insertions.[75] The possible underlying species for each oligotype was determined by basic local alignment search on 16S rRNA sequences as well as NCBI's nr/nt nucleotide collections. The oligotypes were annotated by positions of the minimal entropies with the multiple alignments and the corresponding nucleobase. Position 1 corresponds to the position 300 of the Streptococcus vulneris reference.

Microbiota staining

The frozen microbiota stocks were topped up with 1 mL of autoclaved and sterile-filtered PBS to reduce glycerol toxicity while thawing. Samples were centrifuged at 13,000 xg for 10 min twice, the supernatant removed and the pellets re-suspended in PBS and finally divided into 10 tests. All staining of microbiota samples were performed in a DNase containing buffer (PBS/ 0.2 % BSA/ 25 μg/μL DNase, Sigma Aldrich Cat. No. 10104159001). Staining for human immunoglobulins was performed in 100 μL with 1:50 (v/v) of the detection antibodies: anti-human IgA1 Alexa Fluor 647 (clone: B3506B4, Southern Biotech Cat. No. 9130-31), anti-human IgA2 Alexa Fluor 488 (clone: A9604D2, Southern Biotech Cat. No. 9140-30). The samples were incubated for 30 minutes at 4 ° C and directly topped up with 1 mL of a 5 μM Hoechst 33342 solution (Thermo Fischer Scientific Cat. No. 62249) for another 30 min at 4 °C. For the detection of Spike protein- similar structures, the samples were first incubated in 50 μL containing 0.5 μg rabbit SARS-CoV-2 Spike Neutralizing Antibody (clone: HA14JL2302, Sino Biological Inc. Cat. No: 40592-R001) or Neutralizing Antibody isolated from COVID-19 patients for 15 min at 4 °C then washed with PBS and stained again in 50 μL of the anti-rabbit IgG Alexa647 (7,5μg/ml, Jackson ImmunoResearch Cat. No. 111-606-144) or anti-human IgG PE/ Dazzle™ 594 (2μg/ml; BioLegend Cat. No.: 366920) which was then topped up with 5 μM Hoechst 33342 solution. After Hoechst 33342 staining samples were washed with PBS and centrifuged at 13,000 x g for 5 min. After removal of supernatant, the samples were re-suspended in PBS/ 0.2 % BSA. The samples were transferred to 5 mL round bottom tubes (Falcon, Cat. No. 352063) for acquisition.

Microbiota Flow Cytometry

We used a BD Influx® cell sorter for all cytometric investigations of the microbiota samples. The sheath buffer (PBS) for the instrument was autoclaved and sterile filtered (Steritop® Millipore Express®PLUS 0.22 μm, Cat. No: 2GPT05RE) before each fluidics start

up. The quality of each acquisition was assured by the alignment of lasers, laser delays and laser intensities by Sphero™ Rainbow Particles (BD Biosciences Cat. No. 559123). For sorting, the drop delay was determined prior with Accudrop Beads (BD Biosciences Cat. No. 345249). Samples were acquired with an event rate below 15,000 events and sorted with an event rate below 10,000 events. We always recorded 300,000 Hoechst 33342 positive events. We sorted up to 100,000 events for sequencing directly into Protein Low Bind tubes (Eppendorf Cat. No 022431102), spun down the sample at 17,000 x g and replaced residual sorting buffer by DEPC treated water (Invitrogen Cat. No. 46-2224). The samples were stored in approx. 10 μL at -20 °C until further processing. For subsequent cultivation of bacteria, we sorted directly into PYG medium and transferred the cells directly into a COY anaerobic chamber.

Sequencing from bacterial colonies

For the identification of the bacterial species bound to the neutralizing anti-RBD antibodies, the DNA from 200 μl of the grown bacteria was isolated with ethanol precipitation. The isolated DNA was subsequently amplified by the 16S rDNA specific primers LPW57 and LPW58.[67] In brief, bacterial DNA was amplified with Taq-polymerase (0.005 u/μl, Rapidozym GmbH, Cat. No. GEN-003-1000), 3.12 mM MgCl2 (Rapidozym GmbH), 1 X GenTherm buffer (Rapidozym GmbH), 0.25 mM dNTP mix (Thermo Scientific, Cat. No. R0192) and LPW57 and LPW 58 (1μM, TIB Molbiol) for 35 amplification cycles in a thermocycler. The DNA product was verified by gel electrophoresis and purified with the NucleoSpin Gel and PCR Clean-up Kit (Macherey-Nagel, Cat. No. 740609.50). The concentration of the purified PCR product was adjusted to 5 ng/μl in 15 μl and send to Sanger sequencing by Eurofins Genomics. Sequence identity was determined with the Nucleotide Basic Local Alignment Search Tool (BLAST) provided by NCBI.

Enzyme-linked immunosorbent assay

For the detection of antibody titers in sera, saliva and fecal supernatants 96-well plates were coated with goat anti-human Ig (H+L chain) antibody (Southern Biotech, Cat. No. 2010-01) or goat anti-human IgA Fab (Southern Biotech, Cat. No. 2050-01) antibody for the detection of IgG and IgA respectively. After washing with 1x PBST for 30 seconds, the plates were blocked with 200 μL of 5% PBS/BSA for 1 hour at room temperature. Next, plates were washed 3 times with 200 μL of 1x PBST for 30 seconds at a time. The sera and fecal supernatants were diluted in PBS and 100 μL were added to the plate. Standards were diluted in PBS and applied to the plate: IgA (Genway, Cat. No. E04696) and IgG (Janssen Biotech Inc.,) then the plates were incubated over night at 4°C. After that, plates were washed 5 times with 200 μL of 1x PBST and detection antibodies were applied: anti-human IgG-AP (ICN/Cappel, Cat No. 59289), anti-human IgA-AP (Sigma, Cat.No. A2043), and were incubated for 1 hour at 37°C. Subsequently, the plates were washed 5 times with 200 μL of 1x PBST 100 μL of pNPP (Sigma, Cat. No. N2770) was added to each well. Reactions were stopped by addition of 3M NaOH (Roth: Cat. No. 6771.1). Optical densities were measured on Spectramax (Molecular devices).

Analysis of anti-Spike antibody responses by enzyme-linked immunosorbent assay

To determine the SARS-CoV-2 specific antibody titers, 96-well plates were coated overnight with either 0,5 μg/ml recombinant SARS-CoV-2 Spike S1 Subunit His-tag Protein (R&D 10522-CV) or 0,5 μg/ml recombinant SARS-CoV-2 (2019-nCoV) Spike Protein (RBD, His Tag, Sino biological, Cat. No. 40592-V08B-100) or 0,5 μg/ml recombinant SARS-CoV-2 Nucleocapsid His Protein, CF (RnD Systems; Cat. No. 10474-CV) or 0.5 μg/ml recombinant SARS-CoV-2 Spike RBD protein (flag-his) (Omicron/B.1.1.529) (SanyouBio, Cat. #PNA055) protein or 0,5 μ/ml of RBD peptide ($RBD_{480-496}$: CNGVEGFNCYFPLQSYG; Eurogentek, Cat. No: AS-65619). Plates were washed, blocked and the administration of sera and saliva were done as previously described.[50] To detect S1-specific IgA, a biotinylated anti-human IgA antibody (Southern Biotech, Cat. No. 2050-08) was applied, followed by an incubation for 1 h at room temperature. After washing 5 times with PBST, streptavidin-HRP (Invitrogen, Cat. No. 88-7324-88) was added and after 30 min of incubation at RT and 5 times washing with PBST, Tetramethylbenzidine (TMB) Substrate (Invitrogen, Cat. No. 88-7324-88) was added. The reaction was stopped by addition of 2N H2SO4 (Sigma-Aldrich: Cat. No. 84736). For anti-S1 IgG detection in saliva anti-human IgG-AP (ICN/Cappel, Cat No. 59289) was applied and plates were incubated for 1 hour at room temperature. Subsequently, the plates were washed 5 times with 200 μL of 1x PBST and 100 μL of pNPP (Sigma, Cat. No. N2770) was added to each well. Reactions were stopped by addition of 3M NaOH (Roth: Cat. No. 6771.1). Optical densities were measured on Spectramax plus 384(Molecular devices). OD values were further plotted against respective sample dilutions and areas under the curve (AUC) were quantified using Graphpad Prism 9.3.1. Relative increase in antibody titers for K12 supplementation study was calculated as following: AUC(d14)/AUC(d0)*100.

Flow cytometric assay for analysis of antibody responses against Spike protein

For the detection of "Wuhan" Spike specific immunoglobulins in serum, HEK293T cells were transfected with a plasmid expressing wild-type variant SARS-CoV-2 Spike protein. The next day, the proportion of transfected cells was determined by staining with anti-SARS-CoV-2 Spike Glycoprotein S1 antibody (clone: CR3022, Abcam, Cat. No. ab273073) for 30 min, washing the cells once with PBS/ 0.2 % BSA and subsequent staining with goat anti-human IgG-Alexa-647 (Southern Biotech, Cat. No. 2014-31). Further transfected cells were collected and incubated with sera for 30 min, washed twice with PBS/BSA and stained with goat anti-human IgG Alexa647 (Southern Biotech, Cat. No. 2014-31), and anti-human IgA FITC (Sothern Biotech, Cat. No. 2052-02) in the presence of Fixable Viability Dye eFluor 450 (Invitrogen, Cat. No. 50-112-8817). Cells were washed with PBS/ 0.2 % BSA and either measured directly or fixed in 2 % paraformaldehyde solution for 20 min at 4°C. Samples were acquired on a FACSCanto II (BD Biosciences) or a MACS Quant 16 (Miltenyi Biotec) and analyzed using FlowJo v10 (Tree Star Inc.) analysis software. In the respective fluorescent

channels, geometric mean of fluorescent intensity (MFI) Spike expressing cells and non-expressing cells was quantified and ΔMFI=MFI (S^+)-MFI (S^-) for IgG and IgA was determined. ΔMFI values were further plotted against respective serum dilutions and AUC were quantified using Graphpad Prism 9.3.1.

Epitope mapping for anti-RBD antibodies

Epitope mapping was performed using peptide microarray multiwell replitope SARS-CoV-2 Spike glycoprotein wild type + mutations (JPT Peptide Technologies GmbH; RT-MW-WCPV-S-V02). Microarray was incubated with monoclonal anti-RBD antibodies (final concentration 1 mcg/ml) or mouse fecal supernatants (1:1 dilution) at 30 °C for 1 hour with constant rotation. Slides were washed three times with TBS buffer with 0,05 % Tween-20 and further incubated with anti-rabbit Alexa 647 (Jackson ImmunoResearch Cat. No. 111-606-144), anti-human IgG-Alexa647 (Southern Biotech; Cat. No.: 2040-31), goat anti-Mouse IgA Antibody DyLight® 650 (Bethyl Laboratories; Cat.No.: A90-103D5) at 30 °C for 1 hour. Samples were washed with TBS-T and deionized water, dried by centrifugation. Peptide microarray was analysed using microarray scanner Innoscan 710 (Innopsys). Fluorescence intensities were quantified using ImagePix.

Inhibition of ACE2-RBD interaction

96-well plates were coated with 100ng/ml of human Ace2 protein (Southern Biotech, Cat. No. 2010-01). After washing with 1x PBST for 30 seconds, the plates were blocked with 200 μL of 5% PBS/BSA for 1 hour at room temperature. Next, plates were washed 3 times with 200 μL of 1x PBST for 30 seconds at a time. Fecal supernatants and COVID serum as positive control were diluted in PBS and 100 μL were added to the plate. The plates were incubated at 37°C for 1 h. After that, plates were washed 5 times with 200 μL of 1x PBST and 100 ng/ml of biotinylated RBD (Miltenyi Biotec; Cat No: 130-127-457) was applied and plates were incubated for 1 hour at 37°C. After washing 5 times with PBST, streptavidin-HRP (Invitrogen, Cat. No. 88-7324-88) was added and after 30 min of incubation at RT and 5 times washing with PBST, Tetramethylbenzidine (TMB) Substrate (Invitrogen, Cat. No. 88-7324-88) was added. The reaction was stopped by addition of 2N H2SO4 (Sigma-Aldrich: Cat. No. 84736). Optical densities were measured on Spectramax (Molecular devices). Percentage of inhibition was quantified using the following values: 100% of inhibition corresponded to OD values of blank wells, 0% of inhibition corresponded to the wells where only biotinylated RBD was added.

Generation of Spike SARS-CoV-2 pseudotyped lentivirus

1.2×10^6 293T cells were plated in a 10 cm Petri dish in 10 mL of growth medium. The next day, the cells were transfected with 5 μg pCMV-dR8-2, 6.67 μg pUCHR-IR-GFP, and 3.33 μg of the S-protein coding plasmid using Lipofectamine 2000 (Thermo Fisher Scientific) according to the manufacturer's instruction. Then, 48 h post transfection, supernatant was collected, was filtered through 0.45 μm filters, concentrated using PEG-6000 precipitation, aliquoted, and stored at −80 °C. PVs were titrated on ACE2-expressing 293T cells and assessed by flow cytometry.

Inhibition of lentivirus

Ace2 expressing 293 T cells were plated at 2×10^4 cells/well into 96-well plates the day prior to experiment. Serum samples were serially twice-fold diluted in growth medium saliva samples were diluted 1:10, mixed with S-pseudotyped virus and incubated for 1 h at 37 °C. The mixture was then added to Ace2-293T cells and incubated for 1 day at 37 °C. Infection was determined by flow cytometry.

Lung histology

Lungs for histopathological examination were fixed in 10% neutral buffered formalin for 48 hours at room temperature, washed with PBS and snap-frozen in OCT medium. Lung sections (7 μm) were cut using Cryotome MH560 (Thermo Fisher), were stained with anti-NCP antibody (Thermo Scientific, Cat. No. PA5-119601), followed by secondary anti-rabbit IgG (Jackson ImmunoResearch, Cat No. 111-606-144) and examined using confocal microscope LSM880 (Zeiss). Microphotographs were obtained by LSM880 at 10x magnification and processed using ZEN2 (Zeiss) software. For the evaluation of NCP-APC intensity, the sum of events in APC channel was divided to the square of slide (mm^2) and normalized to secondary only control. For each biological sample 3-5 consecutive slides were analyzed.

Hybridoma generation

P3X63Ag8.653 myeloma cells were grown in RPMI-1640 medium containing 10% fetal bovine serum, 1% penicillin, and streptomycin. Splenocytes from immunized animals were mixed with P3X63Ag8.653 in a 1:1 ratio and washed several times using RPMI-1640 medium. Cells were gently resuspended, followed by the addition of 1 mL of polyethylene glycol (Sigma-Aldrich: Cat.P7181) for 1 minute with constant stirring, followed by 2 mL of RPMI-1640 medium for 2 minutes, and 10 mL of RPMI-1640 medium for 1 minute. Cells were washed and resuspended at a concentration of 2×10^6 /mL in RPMI-1640 medium containing 20% fetal bovine serum, 1% penicillin, streptomycin, 100 μM hypoxanthine, 0.4 μM aminopterin, and 16 μM thymidine, and dispersed on a 96-well plate at 100 μL per well. For 14 days, half of the medium was removed daily and new medium was added. The first colonies were noted on days 6-8 after cell fusion. On day 10, the supernatant in the wells with colonies were analyzed for IgG production and reactivity against RSSL-01370 and RBD-Fc-Tag by ELISA.

Protein gel electrophoresis and Western blotting

48 h bacterial cultures were pelleted and were resuspended in RIPA buffer containing protease inhibitors cocktail (Roche, Cat. No. 11 836 145 001). Samples were sonicated at 50% voltage for 5 cycles of 10 sec pulses followed by 30 sec rest on ice. After sonication glass beads (MP Biomedicals, Cat. No. 6911100) were added as 1/3 of total volume to the bacterial extract. Samples were vortexed for 30 sec followed by chilling on ice for 30 sec (for a total of 5 cycles). Lysates were spun down for 10 min at 20,000 xg and supernatant was collected. For western blot analysis, samples were run on 12% SDS-PAGE under reducing conditions and transferred to PVDF membrane (Bio-Rad, Cat. No. 1620177). SARS-CoV-2 (2019-nCoV) Spike RBD-His Recombinant Protein (Sino Biological, Cat. No. 40592-V08B-100) was used as a positive control. The membrane was blocked by incubation in 5% non-fat milk (Roth, Cat. No. 68514-61-4) in TBST buffer for 1 h at room temperature with constant shaking. The membrane was subsequently hybridized with rabbit neutralizing anti-RBD antibody (Sino Biological, Cat. No. 40592-R001) or human derived RBD neutralizing antibodies in blocking solution for 1h at room temperature with constant shaking. It was then washed in TBST and incubated with anti-rabbit IgG-HRP (Cell signaling, Cat. No. 7074S) or with anti-human IgG-HRP (Southern Biotech, Cat. No. 2040-05) for 1 h at room temperature with constant shaking. SuperSignal West Fempto Maximum Sensitivity (Thermo Fisher scientific, Cat No. 34095) substrate kit was used. The signal was acquired using Chemi Doc imaging system (Bio-Rad).

Mass-spectroscopy analysis of proteins

The protein bands after 1D-PAGE were excised and washed twice with 100 mL of 0.1 M NH4HCO3 (pH 7.5) and 50% acetonitrile mixture at 50°C until the piece of gel becomes transparent. Protein cysteine bonds were reduced with 10mM DTT in 50 mM NH4HCO3 for 30 min at 56 °C and alkylated with 15 mM iodoacetamide in the dark at RT for 30 min. The step with adding DTT was repeated. Then gel pieces were dehydrated with 100 mcl of acetonitrile, air-dried and treated by 10 mcl of 12 mg/mL solution of trypsin (Trypsin Gold, Mass Spectrometry Grade, Promega) in 50 mM ammonium bicarbonate for 15 h at 37°C. Peptides were extracted with 20 mcl of 0.5% trifluoroacetic acid water solution for 30 min with sonication, dried in a SpeedVac (Labconco) and resuspended in 3% ACN, 0.1% TFA. Aliquots (2 mcl) from the sample were mixed on a steel target with 0.3 mcl of 2,5-dihydroxybenzoic acid (SigmaAldrich: Cat. No: 149357) solution (30 mg in 400 mcl of 30% acetonitrile/0.5% trifluoroacetic acid), and the droplet was left to dry at room temperature. Mass spectra were recorded on the Ultraflex II MALDI-ToF-ToF mass spectrometer (Bruker Daltonik, Germany) equipped with an Nd laser. The [MH]+ molecular ions were measured in reflector mode, the accuracy of the mass peak measurement was 0.007%. Fragment ion spectra were generated by laser-induced dissociation, slightly accelerated by low-energy collision-induced dissociation, using helium as a collision gas. The accuracy of the fragment ions mass peak measurement was 1Da. Correspondence of the found MS/MS fragments to the proteins was performed with the help of Biotools software (Bruker Daltonik, Germany) and a Mascot MS/MS ion search.

Protein expression

RSSL-01370 gene was amplified from the genomic DNA of *Streptococcus salivarius K12* using the following primers: 5'- CTC CATATGAATTTACCAAGTCACCATACAAGGG -'3 and 5'- GTGGTCGACATTCACTTTTTCAGTTGCTACACC -'3 and subsequently cloned into pET-21b expression vector containing *NdeI* and *XhoI* restriction sites in Rosetta DE3 (Sigma Aldrich, Cat. No. 70954-3) chemically competent cells. Next, overnight culture of the selected clone was inoculated into 2xTY growth medium containing 100 μg/ml of ampicillin and grown at 30 °C with constant shaking until OD600 reached 0,8. Protein expression was induced by 0,6 mM of IPTG for the next 4 hours at 30 °C. Bacterial lysate was prepared and analysed as described above.

Protein purification

RSSL-01370 protein containing His-tag was expressed in Rosetta DE3 (Sigma Aldrich, Cat. No. 70954-3) cells, bacterial cell suspension was centrifuged at 4500 rpm for 20 min and resuspended in Co2+ Equilibration/Wash buffer containing 300 mM sodium chloride, 50 mM sodium phosphate, 10mM imidazole and protease inhibitors cocktail, pH7,4 (Roche, Cat. No. 11 836 145 001). Sample was sonicated at 50% voltage for 5 cycles of 20 sec pulses followed by 30 sec rest on ice. Lysate was spun down for 10 min at 20,000xg and supernatant containing overexpressed protein was collected. The supernatant was loaded onto HisPur™ Cobalt resin (Thermo Scientific) and purified according to the manufacturer instructions (Thermo Scientific, Cat. No. 89964). Briefly, after loading the protein lysate the column was washed with 10 mM imidazole wash buffer and the uncharacterized protein RSSL-01370 was eluted using 150 mM imidazole elution buffer. Next, overnight dialysis against buffer containing 300 mM sodium chloride and 50 mM sodium phosphate (pH 7,5) was performed for the further applications of the protein.

QUANTIFICATION AND STATISTICAL ANALYSIS

Mann-Whitney or unpaired test was used for statistical evaluation between two groups. Friedman test with Dunn's multiple comparisons for statistical evaluation between multiple groups containing independent variables was used. For the evaluation of NCP protein intensity, the sum of events in fluorescent channel was divided to the square of slide (mm^2) and normalized to intensity derived by staining the consecutive slide with secondary antibody only. For each biological sample 3-5 consecutive slides were analyzed. Wilcoxon matched-pairs signed rank test was used for analysis of data generated in the same individual before and after intervention. To evaluate correlations, Spearman correlation was quantified. Statistical analysis was performed using GraphPad Prism 9.3.1. P-values less than 0.05 were considered statically significant. ns - not significant.

ADDITIONAL RESOURCES

Human participants were enrolled in the study according BNT162-01 study (ClinicalTrials.gov Identifier: NCT04380701) and in the studies approved by the ethics committee at the Charité University Hospital Berlin (EA4/019/21, EA2/200/21, EA2/010/21, EA2/066/20, EA4/188/20 and EA2/002/21) and were performed in compliance with the Declaration of Helsinki.